Topology optimization of conjugate heat transfer systems: A competition between heat transfer enhancement and pressure drop reduction

V. Subramaniam, T. Dbouk, Jean-Luc Harion

Version of Record: https://www.sciencedirect.com/science/article/pii/S0142727X18311342
Manuscript_227db5633b7fa9dfd58e89e7006ce91e

Topology optimization of conjugate heat transfer systems: A competition between heat transfer enhancement and pressure drop reduction

V. SUBRAMANIAM[a,b], T. DBOUK[a,b,], J.-L. HARION[a,b]

[a] *IMT Lille Douai, Energy Engineering Department, 59500 Douai, France*
[b] *University of Lille, 59000 Lille, France*

Abstract

Topology optimization method is developed for a multi-objective function combining pressure drop reduction and thermal power maximization (incompressible flows at low to moderate Reynolds numbers). Innovative optimal designs are obtained, discussed and presented on a Pareto-frontier. The numerical developments (continuous adjoint technique) have been conducted inside an open source CFD platform via the finite volume method. Comparisons have been presented with an optimal design obtained by a Lattice Boltzmann Method from the literature. Finally, this contribution presents and discuss several detailed numerical vitrification steps which are essential to be conducted in topology optimization method when applied with multi-objective functions.

Keywords: Topology optimization; conjugate heat transfer; optimal design; computational fluid dynamics;

Nomenclature

Greek Symbols

Symbol	Description	Unit
α	Pseudo inverse permeability	–
γ	Ratio of thermal diffusivity	–
Γ	Domain boundary	–
η	Design variable	–
ν	Kinematic viscosity	$\mathrm{m}^2 \cdot \mathrm{s}^{-1}$
ρ	Density	$\mathrm{kg} \cdot \mathrm{m}^{-3}$
ϕ_{max}	Maximum volume fraction	%
ω	scalar-valued weight factor	–
Ω	Design domain	–

*Corresponding author
ORCID ID: 0000-0002-9710-4978
Email address: talib.dbouk@imt-lille-douai.fr (T. DBOUK)

Roman Symbols

Symbol	Description	Unit
A	Length of the domain	m
C_p	Specific heat capacity	$\mathrm{J \cdot kg^{-1} \cdot K^{-1}}$
d	Hydraulic diameter	m
D	Thermal diffusivity	$\mathrm{m^{-2} \cdot s^{-1}}$
f_d	Friction factor	$-$
F	Aggregated objective function	$-$
J_f	Dissipated fluid power	W
J_{th}	Recoverable thermal power	W
k	Penalty parameter	$-$
K	Thermal conductivity	$\mathrm{W \cdot m^{-1} \cdot K^{-1}}$
l	Length of the pipe	m
m	Mass flow rate	$\mathrm{kg \cdot s^{-1}}$
$\boldsymbol{n}$	Normal vector	$-$
$nCells$	Number of square elements	$-$
P	Pressure	Pa
T	Temperature	K
$\tilde{T}$	Normalized temperature	$-$
$\boldsymbol{u}$	Velocity vector	$\mathrm{m \cdot s^{-1}}$
$\tilde{u}$	Normalized velocity	$-$
V	Volume of the domain	$\mathrm{m^3}$
$x,\ y$	System of coordinates with dimension	m
$\tilde{x},\ \tilde{y}$	Normalized system of coordinates	$-$

1. Introduction

The term conjugate heat transfer refers to the processes which involve variation of temperature within fluids and solids due to thermal interactions between them. This phenomenon is observed in many industrial thermal equipments like heat exchangers, finned surfaces, microelectronic equipment and heat sinks. The design of such heating or cooling devices involves a consideration of both the heat transfer between different media and the mechanical pumping power spend to overcome the fluid friction in order to move the fluid through the device [1]. In other words, the objective is to increase the heat transfer while keeping the pressure drop as low as possible. Optimizing designs that best manage trade-offs between these two conflicting criteria is currently a very critical issue and has attracted many academic and industrial researchers. On the other hand, rapid product design cycles in development of modern thermal equipment has led to extensive use of automated design and optimization processes. Of the automated optimization techniques that exist in the literature, topology optimization introduced by Bendsøe and Kikuchi [2], can be seen as one of the most promising optimization tool and is presently an active topic of research, development and innovation in the field of heat transfer and fluid flows [3][4].

Topology optimization has its roots in structural design optimization but recently has gained a lot of attention in thermal engineering applications. Originally based on homogenization theory [2], topology optimization has now evolved in different directions which can

be broadly categorized as: density approach [5][6][7], level-set method [8][9][10], topological derivative [11], phase field [12] and evolutionary approaches [13]. These methods in literature have been successfully applied to various problems related to fluid and thermal optimizations. The fundamentals of these techniques are discussed in detail by Sigmund and Maute [14].

TO of heat transfer systems in literature can be broadly classified into three categories: pure heat conduction problems, fluid flow problems and coupled thermal-fluid problems. For heat conduction systems, TO has been found to provide unconventional tree-like optimal structures of high conductivity material for efficient heat evacuation from low conductivity heat generating volumes [15]. Such problems commonly referred as the "volume-to-point" heat conduction problem has been extensively studied in the literature for both 2D [16][17] and 3D [18] cases and recently has also been experimentally investigated [19]. For fluid flow problems, Borrvall and Petersson [20] introduced the concept of TO for Stokes flow by adding a Brinkman penalization sink term into the momentum equation with an objective to minimize the dissipated power in the fluid. This pioneering work was then extended by Gersborg-Hansen et al. [21] to TO for incompressible laminar flows by solving the complete Navier-Stokes equations. After this, several studies were conducted for topology optimization of laminar flows with the objective to either minimize the pressure drop in the channel or to maximize the flow uniformity at the outlet [22][23][24][25]. A detailed review of topology optimization applied to heat transfer and fluid flow problems can be found in [3].

After successful application of TO for heat conduction and fluid flows separately, the next obvious step was to combine these two phenomena to optimize coupled thermal-fluid systems. Early implementations of TO modeled the thermal-fluid systems by combining 2D heat conduction problem with convective heat transfer to the surrounding fluid through Newtons law of cooling by either using a constant heat transfer coefficient [26][27][28] or employing some specific surrogate models [29] to the convective boundaries. In conventional TO methods, it is not easy to clearly define boundary locations in the middle of the process, since they are blurry and constantly changing. Hence, practical implementation of optimal designs obtained from such assumptions (or approximations) is not feasible.

Such limitations can be overcome by adopting a comprehensive conjugate heat transfer approach to optimize thermal-fluid systems. Yoon [30] was among the first researchers to consider TO for a coupled thermo/hydraulic system to optimize for heat dissipating structures under forced convection. A 2D Finite Element Method (FEM) formulation was considered with the objective to minimize the thermal compliance in the domain using the density based Solid Isotropic Material with Penalization (SIMP) [5] approach coupled with method of moving asymptotes (MMA) optimization algorithm, introduced by Svanberg [31]. The author reported several numerical difficulties such as local optima due to high sensitivity of the final design to initialization values. Dede [32] introduced a dual objective function strategy to minimize simultaneously both the mean temperature and the fluid power dissipated in the system with a custom COMSOL/MATLAB solver. A continuous adjoint method for gradient computation and MMA as the optimizer algorithm was used. However, fluid density, heat capacity and viscosity were assumed to be unity in all the examples. Additionally, high values of pressure drop were observed in the system due to undesirable dead-ends in the structure. As a conclusion, the author emphasized on the need of better weighting strategies for multi-objective topology optimization. Lee [33] applied TO to design convective cooling

channels in both 2D and 3D using FEM formulation coupled with discrete adjoint method for sensitivity analysis and Rational Approximation of Material Properties (RAMP) [34] functions for interpolating material properties. Many interesting optimal structures were produced using first a single objective function (mean temperature minimization) and then introducing a bi-objective function (minimizing mean temperature and kinetic energy dissipation) in order to tackle high pressure drop observed in the former case.

Matsumori et al. [35] studied topology optimization for coupled fluid-thermal problem to design heat exchangers under a constant input power using sequential quadratic programming (SQP) algorithm [36] and RAMP-type interpolation functions in the FEM based COMSOL software package. Surprisingly, the authors did not consider the thermal conductivity differences between the solid and fluid regions (i.e. assuming $K_s = K_f$). Kontoleontos et al. [37] extended the TO of coupled fluid-thermal problems to turbulent flows using a finite volume method (FVM) formulation and continuous adjoints for gradient computation coupled with the Steepest-descent optimization algorithm. However, the authors did not solve the temperature field in the solid region by numerically imposing a constant value of temperature. Alexandersen et al. [38] introduced density-based topology optimization for natural convection problems using Boussinesq approximation to design heat sinks and micropumps in a FEM formulation. It is worth to mention that the authors for the first time used a parallelized version of method of moving asymptotes (MMA) algorithm to solve the 3D conjugate heat transfer optimization problem. Koga et al. [39] developed a microchannel heat sink device for electronic cooling using topology optimization for Stokes flows (inertial effects in fluid were not considered) using a FEM formulation and the Sequential Linear Programming (SLP) optimization algorithm. The authors used a RAMP function for interpolating Brinkman penalization term and SIMP for thermal properties. 3D prototypes of numerically obtained 2D optimal structures were fabricated for experimental examination. Marck et al. [40] studied TO of multi-objective heat and mass transfer problems by constructing an overall objective function from linearly weighted two objective functions of pressure drop minimization and thermal power recovery maximization. A FVM based TO formulation with discrete-adjoint method for sensitivity analysis and MMA algorithm was used in their study. The authors presented a Pareto set of optimal solutions for the multi-objective optimization (MOO) of a single pipe with constant wall temperature.

In recent studies, Qian and Dede [41] presented density-based 2D TO of conjugate heat transfer systems with a tangential thermal gradient constraint by using a bi-objective function approach. The authors used the continuous adjoint method to derive gradients of both the objective function and tangential thermal constraint in a FEM formulation. Additionally, they used a RAMP function for interpolating fluid properties and SIMP for thermal properties. The authors emphasized the role of appropriate material interpolation schemes in producing clear fluid/solid designs. Zeng et al. [42] used a multi-stage optimization approach to obtain a non-conventional 2D design of a heat sink under forced convection in COMSOL. 3D representations of the optimal structure was then numerically and experimentally investigated. However, in their formulation, while evaluating heat transfer coefficient in the solid domain, heat conduction was considered only in the height direction (spanwise heat conduction was neglected even though the width of the base is very large as compared to its height). A similar study was performed by Haertal et al. [43] in COMSOL using globally convergent version of MMA (GCMMA) algorithm to optimize the design of a thermo-fluid

heat sink where in 2D results obtained from the topology optimization process were numerically validated in 3D. Lastly, in contrast to density based TO approach, Dugast et al. [44] developed a Level-Set Method (LSM) coupled to adjoint Lattice Boltzman Method (LBM) for topology optimization of thermal fluid flows. The authors presented optimal thermo-fluid designs for fixed pressure drop values with three different cost functions: minimization of mean temperature in the domain, maximization of recoverable thermal power by the fluid, and maximization of the heat exchange with heated solid parts.

Topology optimization applied to CHT systems is an active field of research. During the past decade many numerical techniques have been developed to optimize such systems. Majority of the studies in literature used a FEM formulation and a density approach based on SIMP or RAMP like interpolation scheme for material distribution in the domain. Very few studies investigated the FVM [40][37] and LBM [44][45] discretization techniques for CHT systems. As for the choice of objective function, most of the studies in literature consider either mean temperature minimization in the domain [32][33][35][39][41] or thermal compliance minimization [30][38]. Almost all the studies in literature use a gradient-based optimization algorithm coupled with either discrete or continuous adjoint method for gradient computation. But most importantly, all these numerical techniques in literature, they are too dispersed without enough comparisons in between. Furthermore, to author's knowledge, no benchmark studies exist in this field which hinders the implementation of such studies in real world applications. For example, as most of the studies in literature for CHT systems strive to optimize for heat transfer maximization and pressure drop minimization, it could be interesting to compare different numerical techniques to optimize for some standard academic or industrial configurations on the basis of their respective objective function values. Such studies in future can lead to establishment of best practice guidelines for TO applied to heat transfer and fluid flows.

Another challenge in optimization of CHT systems is to search for optimal designs that can maximize heat transfer in the domain without increasing the pressure drop in the fluid channels (neither blocking the fluid flow). To tackle this issue, some studies optimize only heat transfer enhancement for a prescribed pressure drop values [35][43][44], or optimize only pressure drop with heat transfer performance as a constraint [42]. In reality, optimization of CHT systems falls under the scope of multi-objective optimization (MOO) where the goal is to search for a solution that best manages trade-offs between conflicting criteria and that cannot be transformed into a common measure [46]. Therefore, many researchers adopted the bi-objective function strategy for this task [39][37][32][41][40]. Nonetheless, some studies restricted themselves to Stokes flows [39], whereas others made some unrealistic simplifications in their studies [37][32]. Usually, a bi-objective optimization strategy for CHT systems uses the weighted-sum method to form the overall objective function from the two linearly weighted criteria, a fluid objective (J_f) and a thermal objective (J_{th}), as follows:

$$F = \omega_1 J_f + \omega_2 J_{th} \tag{1}$$

where ω_1 and ω_2 are user-defined scalar-valued weights. The solution of 1 can be unclear, because a single point that optimizes (minimize or maximize) both the objectives simultaneaoulsy usually does not exist. Hence, the solution of such a problem aims at identifying a Pareto set of optimal points also referred as the Pareto frontier [46][47]. Except [40], all

implementations of this bi-objective problem showed the results at a maximum of only two or three optimal points without identifying the Pareto frontier. In other words, most studies in the literature did not exploit the full potential of bi-objective function strategy and consequently did not explore the complete optimal solutions space. On the other hand, as a result of ill-suited boundary conditions opted for the optimization problem Marck et al. [40], reported non physical optimal structures for some designs (i.e. blocking the fluid flow). Precisely speaking, the authors assumed a fixed velocity boundary condition with exactly same value for inlet and outlet, which is an impractical assumption. Finally, one common outcome that can be clearly observed in the literature for such formulations is that whenever the weight of the thermal objective exceeds that of the fluid objective ($\omega_2 > \omega_1$), broken flow paths, dead ends or non-physical artifacts are obtained in the optimal designs [41][40][32]. For this particular reason, no study in literature clearly demonstrated the evolution of optimal design at very high influences of the thermal objective function. This can be due to the formulation itself of the optimization problem, the choice of the objective function or the choice of material interpolation scheme. Nevertheless, such non-physical artifacts are highly undesirable from manufacturing point of view.

In this paper, a multi-objective optimization technique is developed for topology optimization of conjugate heat transfer systems. The design goals are to maximize recoverable thermal power in the domain and minimize the power dissipated by the fluid flow, simultaneously. The two objectives are combined linearly using a linear weighted sum method. In contrast to the commonly used thermal objective functions in literature (thermal compliance or average temeparture in the domain), the recoverable thermal power objective function [40][44] is used in this study as it combines both a tempearture term multiplied by a velocity term. The finite volume method (FVM) is used to solve the coupled thermal-fluid equations over a uniform structured mesh with the open source OpenFOAM CFD software package. A density-based topology optimization approach is adopted and a continuous-adjoint method is used for conducting the sensitivity analysis. The developed topology optimization numerical platform is used to optimize for a fluid channel with single inlet and outlet with constant wall temperature. Several optimal designs are generated for different combination of weighting factors and the Pareto frontier is constructed as the solution of the overall multi-objective optimization problem. The results obtained are compared with those obtained by Marck et al. [40] in terms of objective function values who tackled the similar problem but using a discrete-adjoint method for sensitivity analysis. In addition to this, an another numerical example from literature [44] is solved in order to compare the optimal designs obtained from the present TO numerical platform to the adjoint LBM coupled to LSM based TO in terms of objective function values.

To summarize, the main novelty of this work can be summed up as follows:

– Multi-objective topology optimization technique of CHT systems is developed methodologically by linear combination of two objective functions for pressure drop reduction and heat transfer enhancement which is a very critical task in terms of producing physically realistic optimal designs as it induces severe numerical difficulties in the overall optimization problem due to the physical contradiction behind enhancing heat transfer by material insertion combined to reduction in pressure drop.

– The developed TO technique produces Pareto optimal solutions with more realistic and physically logical structures even at higher influence of thermal objective function without any dead ends or blocked fluid flow which were never reported before in the literature, to authors' knowledge.

– An in-depth analysis of the obtained optimal fluid channel designs in terms of convergence study, performance evaluation, local analysis of the results at the domain boundaries and order of magnitude analysis of the objective functions is presented for the first time, to authors' knowledge.

– Finally, a detailed comparison of the performance of different topology optimization approaches for optimizing conjugate heat transfer systems is presented. In that purpose, the results produced from the **present FVM coupled to density approach based** TO solver are compared to other studies in literature [40] (**FVM coupled to density approach based**) and [44] (**LBM coupled to level-sets based**) by solving identical CHT TO problems for the same objective function. Better optimal designs are obtained in the current study and justified in terms of the objective function values.

The rest of the article is organized as follows: Section 2 presents the mathematical formulation of the inequality constrained topology optimization problem for conjugate heat transfer systems describing the multi-objective function approach, material interpolation techniques, continuous adjoint formulation and numerical implementation of the problem. Section 3 presents the results obtained for the TO problem with an in-depth numerical analysis of the optimal designs obtained and influence of several physical and numerical parameters and finally in section 4, conclusions are drawn and some perspectives are proposed for the near future.

2. Topology optimization for conjugate heat transfer systems

Topology optimization (TO) addresses the fundamental engineering problem of placing different materials within a given design domain that obeys a predefined design objective. Mathematically, the goal of TO is to maximize or minimize some objective function while taking into account one or more constraints. Figure 1 represents the design domain Ω and boundary conditions for the conjugate heat transfer topology optimization problem. The domain under consideration is a square of length $A(m)$ and has one inlet (Γ_{in}) and one outlet (Γ_{out}) of length $A/5$. The inlet flow has a prescribed parabolic velocity profile $\boldsymbol{u}_{in}$ and a constant temperature of $T_{in} = 273$ K. The outlet flow has a zero gradient boundary condition for both velocity and temperature. The top and bottom walls (Γ_{w}) are maintained at a constant temperature of $T_w = 283$ K. All other boundaries (Γ_{ad}) are adiabatic. The boundaries Γ_{w} and Γ_{ad} are subjected to no-slip velocity boundary condition. The fluid under consideration is assumed to be incompressible, Newtonian and under steady-state laminar flow regime with kinematic viscosity of $6.6 \cdot 10^{-6}\ m^2\ s^{-1}$. The Reynolds number varies between Re=3 and Re=100, evaluated on the basis of characteristic length of $A/5$ and a varying inlet fluid velocity. The thermal diffusivity ratio ($\gamma = D_s/D_f$) between solid and fluid material is 10. The amount of the fluid material is limited by restricting the ratio of its effective volume to the total domain volume, given by ϕ_{max} (the maximum allowed

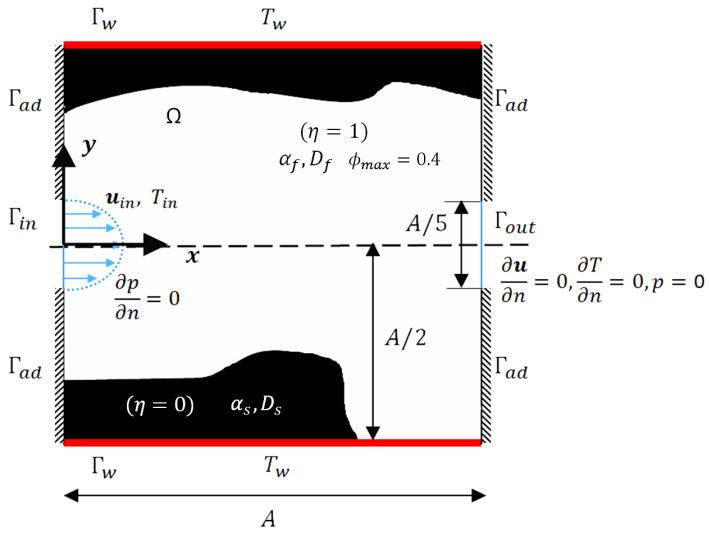

Figure 1: 2D design domain and boundary conditions for conjugate heat transfer topology optimization problem.

relative quantity of fluid material) and for the current problem, $\phi_{max} = 0.4$. As is the case with OpenFOAM CFD software package, 2D simulations here are performed on a 3D mesh with one cell width of 0.005 m in the third direction. Thus, the described design domain represents a typical channel flow with constant wall temperature.

A local design variable field η is introduced which will be used as a characteristic function to represent the optimal material distribution in the design domain. The design variable varies continuously from 0 to 1 in each cell in the domain where $\eta = 0$ represents a solid material and $\eta = 1$ represents a fluid material. The aim of the current topology optimization process is to find an optimal distribution of design variables η in the design domain in order to minimize an objective function F. Mathematically, the above TO problem can be expressed as follows:

Minimize:

$$F(\boldsymbol{u}, p, T, \eta) \tag{2a}$$

subject to:

$$\nabla \cdot \boldsymbol{u} = 0 \tag{2b}$$

$$(\boldsymbol{u} \cdot \nabla)\boldsymbol{u} = -\nabla p + \nabla \cdot (\nu \nabla \boldsymbol{u}) - \alpha(\eta)\boldsymbol{u} \tag{2c}$$

$$(\boldsymbol{u} \cdot \nabla)T = \nabla \cdot (D(\eta)\nabla T) \tag{2d}$$

$$\frac{1}{V} \sum_{j=1}^{nCells} \eta_j \leq \phi_{max} \tag{2e}$$

where F is the objective function to be minimized, subjected to the state equations for incompressible steady-state Navier-Stokes (N-S) equations coupled with heat transfer (2b-2d) and an inequality volume constraint on the fluid material (2e). V is the total volume of

the square domain and $nCells$ is the number of square elements used to discretize uniformly the 2D domain in a Cartesian frame of reference. $\boldsymbol{u}$, p, T and ν represents the fluid velocity vector, pressure, temperature and the fluid kinematic viscosity, respectively. The objective function F is explicitly dependent on velocity, pressure and temperature field and also implicitly dependent on the local design variable η. Here, α is the inverse permeability or the friction coefficient which is linked to the local design variable (η) through an interpolation function. Similarly, in the energy equation the effective thermal diffusivity (D) is dependent on the local design variable (η) via an interpolation function such that:

$$(\alpha(\eta), D(\eta)) = \begin{cases} (\alpha_s, D_s), & \text{if } \eta = 0 \text{ (solid material)} \\ (\alpha_f, D_f), & \text{if } \eta = 1 \text{ (fluid material)} \end{cases} \tag{3}$$

The Brinkman penalization approach [48, 49] is applied here to penalize the momentum equation by a source term in order to account for the presence of immersed solid regions in the fluid flow domain. The main idea behind this approach is to force a zero velocity inside the stationary solid material regions by means of the Brinkman penalization source term ($-\alpha\boldsymbol{u}$) in equation (2c) when α tends to a very large value of the order $O(10^5)$. The

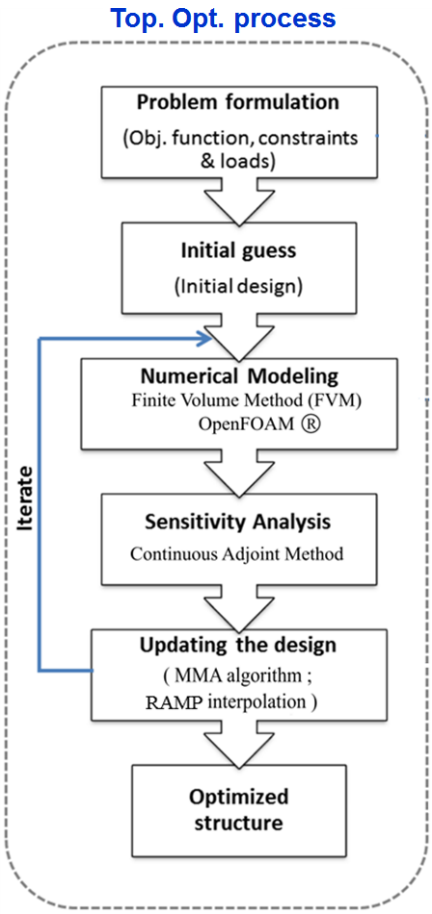

Figure 2: The topology optimization process.

above optimization problem of equation 2 requires some specific numerical algorithms and

TO methods to be used in order to find an optimum. The complexity of any optimization problem depends on various factors like number of design variables involved, degree of convexity/non-convexity and linearity/non-linearity of the equations and the associated numerical difficulties. Therefore, choosing an efficient TO technique and an equally reliable optimization algorithm is very important to ensure a stable convergence to an optimum solution. Figure 2 presents the basic steps involves in the present TO process.

2.1. Interpolation functions

The optimal solution of a topology optimization problem requires discrete variable values only (well defined design) of the design variables η (for example 0 for solid regions and 1 for fluid regions). However, with the continuous medium formulation makes it difficult to reach directly discrete design variables. The density based TO approach [50], overcome this problem by introducing a continuous design field, $\eta(\boldsymbol{x})$ which replaces the discrete variables with continuous ones that is then modified iteratively by a material interpolation technique to reach only discrete design variables. As a result, the friction coefficient (α) and effective thermal diffusivity (D) change with η through the following Rational Approximation of Material Properties (RAMP)-type [34] interpolation functions as following:

$$\alpha(\eta) = \alpha_s + (\alpha_f - \alpha_s)\eta\frac{1+k}{\eta+k} \tag{4a}$$

$$D(\eta) = D_s + (D_f - D_s)\eta\frac{1+k}{\eta+k} \tag{4b}$$

with $0 \leq \eta \leq 1$ and $k > 0$. This penalty parameter k governs the shape of the functions $\alpha(\eta)$ and $D(\eta)$. The above material interpolation scheme interpolates the value of α between the two extrema of $\alpha_f \approx 0$ and $\alpha_s \approx \infty$. Thus, in the fluid domain, the Brinkman penalization term $\alpha\boldsymbol{u}$ approaches zero to recover the classical Navier-Stokes equation in 2c. Conversely, in the solid domain , the friction coefficient α has a very large value, which makes the local velocity approach zero. In the present work, $\alpha_f \approx 0$ and $\alpha_s \approx 10^5$.

2.2. Multi-objective optimization

Efficient optimization of CHT systems requires to optimize for a thermal objective and a fluid objective, simultaneously in order to reach a design that best manages trade-off between the two criteria. A trade-off here means one objective can be improved only by worsening the other one. The solution of such a multi-objective optimization (MOO) problem is not a single point but a set of optimal points (multiple solutions) referred as the Pareto frontier. Thus MOO based on Pareto optimality is divided into two steps: In the first step, the set of pareto optimal solutions is identified and in the second step the final design is selected by a human decision maker based on subjective preferences. The weighted sum method based on linear combination of the objective functions is a suitable method for identifying the Pareto front [51].

For the current problem the multi-objective function is constituted of two objectives inspired from [40][24]. The fluid objective function J_f is to minimize the power dissipated by

the fluid flow in the domain Ω and can be calculated from the total pressure losses through the overall domain boundaries Γ as the following:

$$J_f(\boldsymbol{u}, p) = -\int_\Gamma \Big(p + \frac{1}{2}|\boldsymbol{u}|^2\Big)\boldsymbol{u}\cdot\boldsymbol{n}\ d\Gamma \tag{5}$$

The thermal objective function J_{th} is to maximize the recoverable thermal power from the domain through the inlet and outlet flow boundary conditions. The net thermal power is evaluated as follows:

$$J_{th}(\boldsymbol{u}, T) = \int_\Gamma (\rho C_p T)\boldsymbol{u}\cdot\boldsymbol{n}\ d\Gamma \tag{6}$$

where $\boldsymbol{n}$ is the unit vector normal to the boundary Γ. The weighted sum method or the aggregated objective function is used to linearly combine the two objective functions. As a prerequisite to this approach, the two objective functions are normalized to avoid the huge differences in their numerical values corresponding to two different scales. One simple yet efficient way of normalizing is to divide the objective functions by their respective extrema [47]. The extreme value for each objective function is found independently upon solving the optimization problem (Eqn. 2) for two cases separately: minimizing J_f and maximizing J_{th}, respectively. Finally, the aggregated objective function (F) for the current MOO problem formed from the linear combination of the two normalized objective functions, $\tilde{J_f}$ and $\tilde{J_{th}}$, can be described as follows:

$$F(\boldsymbol{u}, p, T) = (1-\omega)\tilde{J_f} - \omega\tilde{J_{th}} \tag{7}$$

where ω is a scalar-valued weight factor emphasizing the degree of influence or priority of each objective function ($\omega \in (0, 1)$). The thermal objective $\tilde{J_{th}}$ is negatively weighted as it has to be maximized (since the overall F is to be minimized). The weighted-sum approach can obtain the convex part of the Pareto front by progressively varying the weight factor values in the aggregated objective function formulation [46].

2.3. Sensitivity analysis - The continuous adjoint method

In gradient-based TO, the derivative of the objective function with respect to the design variables is required by the optimization algorithm to solve for the design variables in each cell satisfying the optimization problem in equations (2). The adjoint method, either discrete or continuous, provides an efficient option for calculating the sensitivity field of the objective function, $dF/d\eta_j$ and has been applied in many different TO problems (i.e. see [3][37][52][45]). In contrast to Marck et al. [40] who applied a discrete adjoint method, a continuous adjoint method is used here for sensitivity field computation. For this, the adjoint equations and the corresponding boundary conditions are first derived in their analytical form and then discretized to obtain the adjoint equations.

The original constrained optimization problem of Eqn. 2 can be transformed into an unconstrained optimization problem by introduction of a Lagrange function L (also reffered as the augmented objective function) [53]. Reformulating the objective function as follows:

$$L = F + \int_\Omega (\boldsymbol{u}_a,\ p_a,\ T_a)R\ d\Omega \tag{8}$$

where the Lagrange multipliers $\boldsymbol{u}_a,\ p_a$ and T_a are the adjoint velocity, adjoint pressure and the adjoint temperature, respectively, and $R = (R_1, R_2, R_3, R_4, R_5)^T$ represent the state equations for the incompressible steady-state Navier-Stokes equations coupled with heat transfer.

As the objective function is dependent on both the topology (via the design variable η) and the flow field ($\boldsymbol{u},\ p,\ T$), the total variation of the objective function with respect to a design change can be expressed as:

$$\delta L = \delta_\eta L + \delta_{\boldsymbol{u}} L + \delta_p L + \delta_T L \tag{9}$$

Now, if the adjoint variables ($\boldsymbol{u}_a,\ p_a,\ T_a$) are chosen in such a way that the variation of the objective function w.r.t flow field variables vanishes,

$$\delta_{\boldsymbol{u}} L + \delta_p L + \delta_T L = 0 \tag{10}$$

then the sensitivities can be evaluated directly as follows:

$$\delta L = \delta_\eta L = \delta_\eta F + \int_\Omega (\boldsymbol{u}_a,\ p_a,\ T_a)\delta_\eta R\ d\Omega \tag{11}$$

The total variation can also be expressed as $\delta L = \dfrac{\partial L}{\partial \eta}\delta\eta$. Thus, from Eqn. 11, the gradient of the objective function with respect to the design variable η for each cell i can be further simplified as:

$$\frac{\partial L}{\partial \eta_i} = \frac{\partial F}{\partial \eta_i} + \int_\Omega (\boldsymbol{u}_a,\ p_a,\ T_a)\frac{\partial R}{\partial \eta_i}\ d\Omega \tag{12}$$

In density based TO approach, the design variable η is used as a variable to represent a continuous transition between the two materials and as a result there is no explicit dependence of the objective function on the design variable ($\partial F/\partial \eta_i = 0$), hence the above equation can finally be written as:

$$\frac{\partial L}{\partial \eta_i} = \int_\Omega (\boldsymbol{u}_a,\ p_a,\ T_a)\frac{\partial R}{\partial \eta_i}\ d\Omega \tag{13}$$

If the adjoint variables ($\boldsymbol{u}_a,\ p_a,\ T_a$) are known, the topological sensitivities i.e. the gradient of the objective field w.r.t the design variable in each cell can be easily evaluated from the above equation. For this, the governing equations for adjoint variables needs to be derived along with their appropriate boundary conditions which then are solved along with the primal flow field equations to get the adjoint variables.

2.3.1. Continuous adjoint equations and boundary conditions

The requirement of vanishing of variation of Lagrange function L w.r.t the flow field variables (Eqn. 10) serves as the starting point for derivation of adjoint system of equation:

$$\delta_{\boldsymbol{u}} F + \delta_p F + \delta_T F + \int_\Omega (\boldsymbol{u}_a,\ p_a,\ T_a)\delta_{\boldsymbol{u}} R\ d\Omega + \int_\Omega (\boldsymbol{u}_a,\ p_a,\ T_a)\delta_p R\ d\Omega + \int_\Omega (\boldsymbol{u}_a,\ p_a,\ T_a)\delta_T R\ d\Omega = 0 \tag{14}$$

Starting from Eqn. 14, calculating the derivatives of the state equations R w.r.t $\boldsymbol{u}$, p and T; integration by parts; decomposition of the cost function F into contributions from the domain boundary $\Gamma = \partial\Omega$ and the interior Ω and using the Gauss divergence theorem to transform volume integrals to surface integrals, the final adjoint equations are derived. The detailed development of the adjoint equations and the associated boundary conditions can be found in the works of Othmer [24] and Hinterberger et al. [54]. The only addition here is the energy equation due to the coupling of heat transfer with fluid flow. The complete continuous adjoint equation system for the optimization problem described in Fig. 1 is as follows:

Continuous adjoint equations:

$$\nabla \cdot \boldsymbol{u} = \frac{\partial F_\Omega}{\partial p} \tag{15a}$$

$$-2\mathbf{E}(\boldsymbol{u}_a) \cdot \boldsymbol{u} = -\nabla p_a + \nabla \cdot (2\nu \mathbf{E}(\boldsymbol{u}_a)) - \alpha(\eta)\boldsymbol{u}_a + T\nabla T_a - \frac{\partial F_\Omega}{\partial \boldsymbol{u}} \tag{15b}$$

$$-\boldsymbol{u} \cdot \nabla T_a = \nabla \cdot (D(\eta)\nabla T_a) - \frac{\partial F_\Omega}{\partial T} \tag{15c}$$

with rate of strain tensor $\mathbf{E}(\boldsymbol{u}_a) = \frac{1}{2}(\nabla \boldsymbol{u}_a + (\nabla \boldsymbol{u}_a)^{\mathrm{T}})$. The system of adjoint equations are mathematically very similar in structure to the primal N-S equations except that the adjoint convection is upstream to the primal flow due to the minus sign and there are additional volumetric source terms when there is any contribution from interior of the domain Ω to the objective function F. It should be noted that the adjoint variables ($\boldsymbol{u}_a$, p_a, T_a) do not have any physical meaning to them unlike their primal counterparts ($\boldsymbol{u}$, p, T). Depending upon the primal boundary conditions for the N-S equations coupled with heat transfer (described in Fig. 1), the adjoint boundary conditions are derived. The adjoint boundary conditions for the current problem of single channel flow with heat transfer are as follows:

Adjoint boundary conditions for inlet and wall:

$$\boldsymbol{u}_{at} = 0 \tag{16a}$$

$$u_{an} = -\frac{\partial F_\Gamma}{\partial p} \tag{16b}$$

$$\boldsymbol{n} \cdot \nabla p_a = 0 \tag{16c}$$

$$T_a = 0 \tag{16d}$$

Adjoint boundary conditions for outlet:

$$\boldsymbol{u}_a \cdot \boldsymbol{u} + u_{an}u_n + \nu(\boldsymbol{n} \cdot \nabla)u_{an} + TT_a + \frac{\partial F_\Gamma}{\partial u_n} = p_a \tag{17a}$$

$$u_n \boldsymbol{u}_{at} + \nu(\boldsymbol{n} \cdot \nabla)\boldsymbol{u}_{at} + \frac{\partial F_\Gamma}{\partial \boldsymbol{u}_t} = 0 \tag{17b}$$

$$u_n T_a + D(\eta)(\boldsymbol{n} \cdot \nabla T_a) + \frac{\partial F_\Gamma}{\partial T} = 0 \tag{17c}$$

The continuous adjoint equations and the associated boundary conditions described above are generic in nature and can be customized for any objective functions. On closer observation, it can be seen that there are seven derivative of the objective function, highlighted in red in the above equations, required to complete the adjoint system of equations.

A key element of the adjoint method is the choice of correct boundary conditions and their customization for the current objective function. In other words, the complete adjoint system needs to be reformulated on changing the objective function form due to the seven terms described above. This characteristic of adjoint-based TO makes it almost impossible to automate the TO numerical platform to tackle wide range of objective functions. Nevertheless, the two objective functions in the present study in Eqn. 5 and Eqn. 6 are evaluated only on the domain boundary Γ and there is no contribution from the domain interior ($F_\Omega = 0$). As as result the three derivatives in the Eqn. 15 can be neglected and the remaining derivatives are calculated by partial differentiation of the multi-objective function Eqn. 7 with respect to p, u_n, $\boldsymbol{u}_t$ and T. These derivatives are then fed into the adjoint boundary conditions Eqn. 16 and Eqn. 17 to get the specific continuous adjoint equation system for the current multi-objective function.

2.4. Numerical methods and algorithm implementation

The Finite Volume Method (FVM) is used to discretize spatially the system of PDE's in (2) over the computational domain in order to compute the fluid flow and temperature fields. The finite volume formulation for coupled thermo-fluid problems was rarely applied in the literature [40][37]. The SIMPLE algorithm [55] is applied to solve the pressure-velocity coupling for the steady-state incompressible fluid flow under consideration coupled to the heat equation. The SIMPLE algorithm reformulates the initial N-S equations into a momentum prediction and a pressure correction that are solved iteratively such that the resulting velocity field satisfies well the continuity equation (2b). The SIMPLE algorithm can be easily extended to solve the adjoint equations as the primal and adjoint system of equations share similar structure. This facilitates complete gradient computation with just two solver calls for primal and adjoint equations, respectively.

The method of moving asymptotes (MMA) [31, 56] is used as the optimization algorithm in the current TO problem. This gradient-based algorithm is based on logarithmic-based convex separable approximations applied to the objective function and its constraints. It is widely used in literature for various structural and multidisciplinary topology optimization problems [20][32][38][40][30]. A detailed analysis about the general performance of this algorithm can be found in [57].

Density and sensitivity filtering methods are often used in topology optimization to obtain mesh-independent and checkerboard-free solutions [58] with length-scale control. In this work, a density filter is used with a filter radius of 1.51 mm. Initially introduced by Bruns and Tortorelli [59], a density filter modifies the element (or mesh cell) density as a function of the densities in a specified neighborhood of an element [60]. The steady state results in this study are obtained over a 100×100 structured uniform square cells mesh. All the above mentioned components of this TO formulation are implemented in the OpenFOAM C++ open source CFD package.

The above topology optimization solver implementation can be summarized as the following:

1. Provide an initial guess for the design variables η.

2. Solve the governing equations to obtain the flow ($\boldsymbol{u},\ p$) and temperature field (T).

3. Compute the multi-objective cost function $F(\boldsymbol{u}, p, T)$.

4. Calculate the sensitivities using the continuous adjoint formulation.

5. Use the computed sensitivities, fluid flow and temperature distribution to update the design variables using the Method of Moving Asymptotes.

6. If the overall convergence/stopping criterion is not reached, go back to step 1 using the new design variables.

The applied overall convergence/stopping criterion is based on both: the design variable changes in the last iteration to be negligible, and the squared-norm of the Karush-Kuhn-Tucker (KKT) conditions to be less than a very small positive value $\ll 1$.

3. Results

This section presents the optimal numerical designs obtained for multi-objective topology optimization of the conjugate heat transfer (CHT) problem described in fig. 1. In non-dimensional analysis, the temperature and velocity field magnitude values will be normalized as the following:

$$\tilde{T} = \frac{T - T_{in}}{T_w - T_{in}} \tag{18}$$

$$\tilde{u} = \frac{|\boldsymbol{u}|}{|\boldsymbol{u}_{in}|_{max}} \tag{19}$$

where T_{in} is the fluid temperature at the inlet boundary, T_w is the temperature at the top and bottom walls boundaries Γ_w and T is the local steady state temperature in the domain. Similarly, $|\boldsymbol{u}_{in}|_{max}$ is the maximum fluid velocity at inlet and $|\boldsymbol{u}|$ is the local steady state velocity magnitude (in $m\ s^{-1}$) in the domain.

3.1. Optimal designs for CHT systems

The domain under investigation is a square channel with single inlet and single outlet subjected to constant wall temperature on top and bottom walls. The eastern- and western-side walls are considered adiabatic (see figure 1). The multi-objective TO problem is solved for different values of ω in the range of 0 to 1 to take into account the influence of the two participating objective function depending on the value of the scalar weight factor, ω. For the problem description in fig. 1, figure 3 shows various distinct optimal designs obtained by progressively increasing the value of ω along with the corresponding normalized velocity magnitude and normalized temperature fields for the obtained optimal designs.

Here dark regions represents solid material and light regions correspond to fluid material, as demonstrated in fig. 1.

For $\omega = 0$ (Fig 3(a)), when there is no contribution from the thermal objective function J_{th} to F and thus the only objective is to minimize the fluid power dissipation, the optimal design obtained is a direct fluid curved channel symmetric in both x and y directions connecting the inlet to the outlet with an increase of cross section (compared to inlet and outlet) thus corresponding to a decrease of pressure drop. As a result, the value of fluid objective J_f is minimum for this design. In other words, it is the best possible design for least pressure drop under the current flow conditions. Additionally, the recoverable thermal power from the domain in this case is about 0.3 Watts.

Subsequently, the optimal two designs obtained at $\omega = 0.3$ and $\omega = 0.5$ add more priority to increases the thermal objective J_{th} permitting some increase in the J_f value, but the continuity, momentum and energy conservation equations must be always satisfied so that the obtained design/structure to be acceptable and feasible. Note that the velocity fields for the first two structures are almost similar, however for $\omega = 0.5$, the optimal structure tries to slightly increase the velocity at the outlet-center by forming a converging shape at the exit (with the continuity constraint being well preserved as will be shown in Section 3.3). Indeed, this effect is more pronounced for the next structure with $\omega = 0.7$ where the structure becomes narrower to increase more the velocity value at outlet-center. In fact, the thermal objective function J_{th} (refer equation 6) has contribution from both the temperature and the normal component of velocity at outlet. Hence the designs until now can be seen as modifying the straight fluid connection in a way to increase the velocity at the outlet in the flow direction.

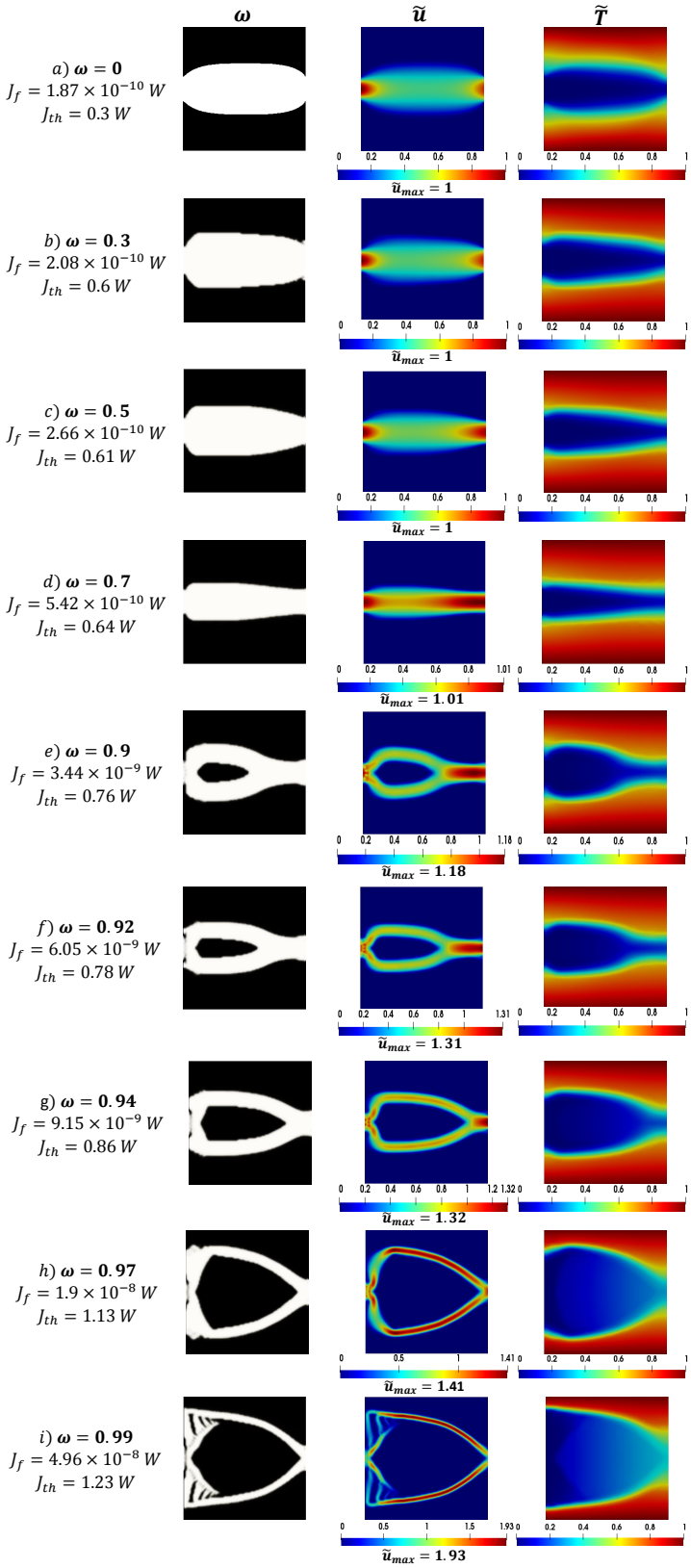

Figure 3: Optimal designs of conjugate heat transfer systems: Starting from fluid objective J_f minimization ($\omega = 0$) to thermal objective J_{th} maximization ($\omega = 0.99$).

Adding more priority in the overall objective function F to maximize J_{th} at $\omega = 0.9$, the fluid flow channel is split into two upper and lower fluid paths with solid material core created in between. The TO solver is trying to place the fluid regions in a way to gain heat from upper and lower solid material regions (knowing that the thermal conductivity of solid is 10 times higher than that of the fluid). Moreover, upon increasing ω, the two divided fluid channels are gradually becoming narrower to rush the exiting fluid where solid material is added at the outlet boundary without totally blocking the fluid flow passage (thus respecting the continuity and momentum conservation equations). At $\omega = 0.94$, 0.97, 0.99, there is a simultaneous increase of both temperature and velocity values at the outlet. These influences will be analyzed in more details in a local analysis of results at the outlet boundary in Section 3.4.2.

At $\omega = 0.99$, the optimal design obtained owns an increased recoverable thermal power of 1.23 W, constituting a significant increase of 310 % as compared to the design obtained at $\omega = 0$. However, this 3-times increased thermal power recovery comes at a cost of 6-times increased fluid power dissipation. Moreover, at very high values of ω, no broken flow paths, fluid flow blockage, dead ends or non-physical artifacts are observed in this work which is a major new finding compared to previous designs obtained previously in the literature which for multi-objective TO of coupled fluid flow and heat transfer problems [17][41][32].

The Pareto frontier in multi-objective optimization problems is an indispensable tool which illustrates the complete solution space and provides the designer with freedom to choose from suitable designs depending on her/his own needs. Unfortunately, most studies in the literature, which dealt with multi-objective TO of CHT systems, did not present this important aspect of the Pareto frontier.

At $\omega = 1$, when there is absolutely no contribution from the objective function J_f, the optimal structure becomes very complex (see Fig. 4) due to an extremely increased non-linearity in the overall optimization problem inducing high numerical instabilities that require large computing efforts to solve at a good precision. This is due to the form of the J_{th} objective function itself that combines both a temperature (T) term multiplied by a velocity term ($\boldsymbol{u} \cdot \boldsymbol{n}$). In fact most studies in the literature, to avoid these numerical complexities, consider either a simple thermal objective that is a function of the temperature field T only or by introducing a convection source term in the energy equation. However, such objective function simplification leads to very limited design space exploration (if not unrealistic designs are obtained), because the fluid flow contribution can not be neither neglected ($\boldsymbol{u} \cdot \boldsymbol{n} = 0$) nor assumed at a velocity value of unity ($\boldsymbol{u} \cdot \boldsymbol{n} = 1$) due to the CHT nature of the system.

Upon comparing the designs obtained in the present study to those obtained by Marck et al. [40], who applied the same objective function F and studied the same problem for single pipe with constant wall temperature with identical flow and thermal conditions (but with discrete adjoint system applied, and $u_{inlet} = u_{outlet}$ imposed boundary condition), the following important critical points can be observed (see Figure 5):

- Upon increasing the weighting factor ω, Marck et al.[40] observed the splitting of the fluid channel at a very lower value $\omega = 0.06$.
- Nonphysical designs like broken flow paths at $\omega = 0.75$ and total fluid flow blockage at $\omega > 0.75$ were reported.

– Finally, the magnitude for the recoverable thermal power objective function J_{th} of the order of magnitude of 10^{-5} W was surprisingly reported.

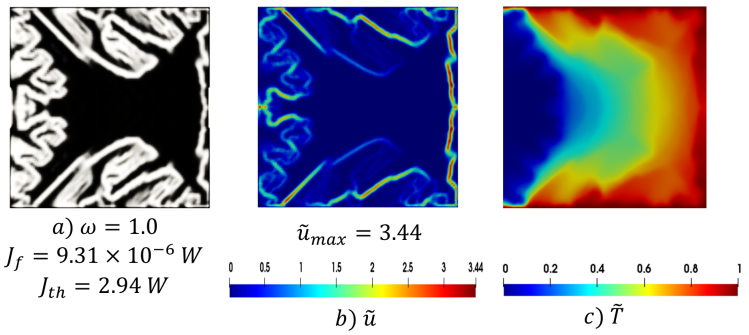

Figure 4: Optimal design obtained by $\omega = 1$.

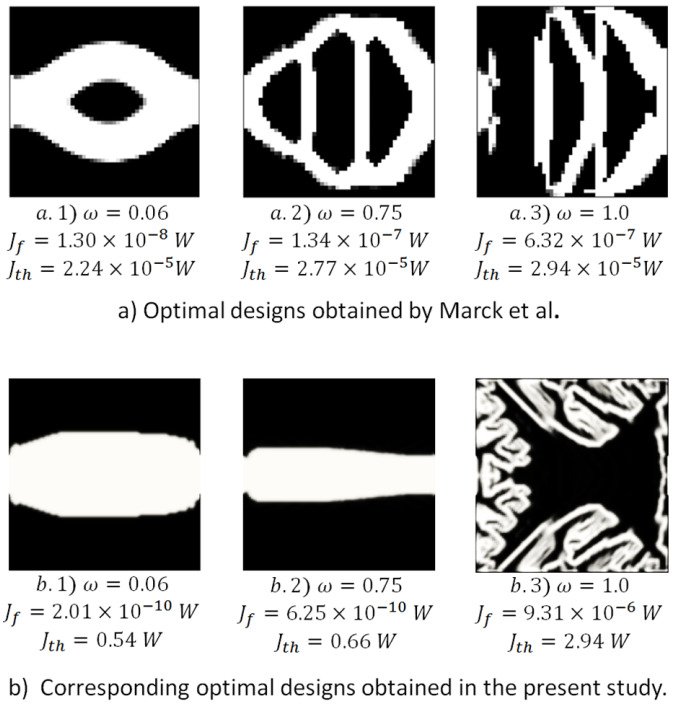

Figure 5: Optimal designs for single pipe with constant wall temperature: a) Obtained by Marck et al.[40] and b) Corresponding designs obtained in the present study.

The above three differences in the two studies will be analyzed in detail in the later sections (refer Section 3.3, Sec. 3.4.2 and Sec. 3.5). Apart from these three major differences, another peculiar observation for the result at $\omega = 1.0$ obtained by Marck et al. [40] is that the order of magnitude of the fluid objective function J_f is same for the two designs at $\omega = 0.75$ and $\omega = 0.1$ even when the flow is totally blocked in the latter. If there is no fluid connection between inlet and outlet at $\omega = 1.0$, as observed by the authors, the pressure drop should

have been very high and consequently the value of J_f should have been significantly higher as compared to other designs. Conversely, in the present study, the order of magnitude for the optimal design at $\omega = 1.0$ (where there is still a fluid connection between inlet and outlet) is much higher to that of $\omega = 0.99$ ($10^{-6} \gg 10^{-8}$) as a result of complex fluid channels in the design (refer Figure 3 and 5).

3.2. Pareto optimal points for multi-objective topology optimization

Figure 6 represents the Pareto frontier obtained for the present multi-objective TO problem for a conjugate heat transfer system. It is obtained by solving the MOO problem for several different weighting factor values between 0 and 1. All the optimal points presented here were verified for convergence satisfying the equality (governing equations) and the inequality (max allowed volume of fluid material) constraints of the TO problem (refer Eqn. 2).

A critical feature of the weighted sum method for MOO is that it can generate the convex part of the Pareto frontier [46]. Hence, the convex shape of the obtained Pareto front (Fig. 6) for the present TO problem is another confirmation of the optimality of the solution points presented here. This Pareto frontier curve constitutes a decision maker tool to select an optimal design based on the needs of the user (i.e. available pumping power, material properties, maximum allowed temperature, etc).

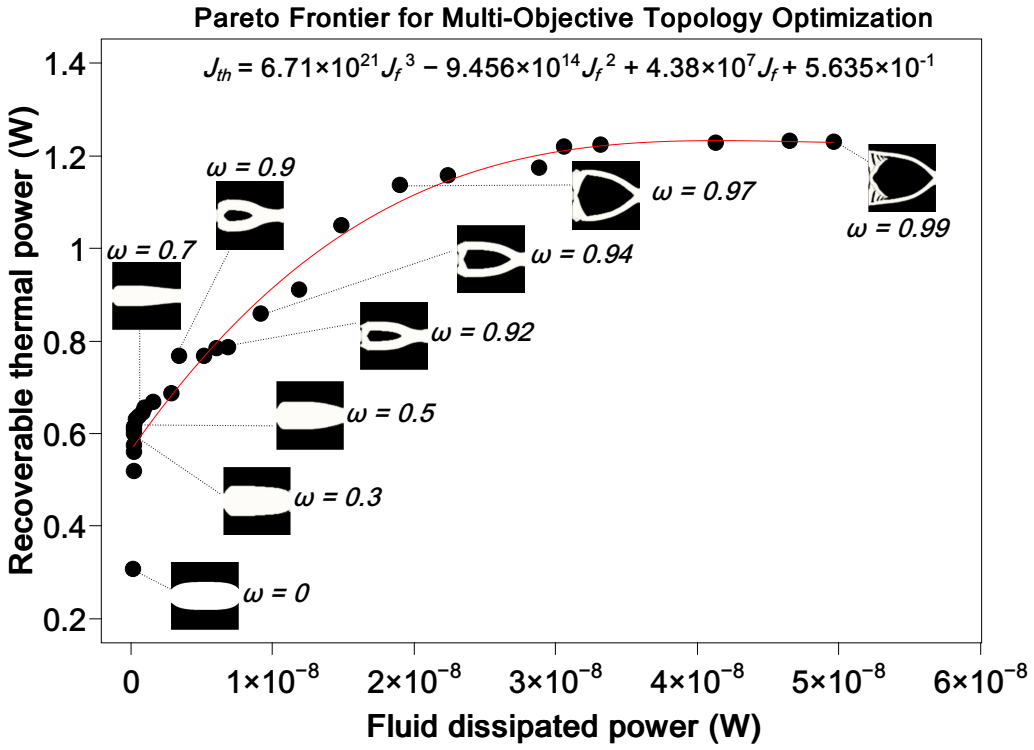

Figure 6: Pareto frontier for multi-objective topology optimization of conjugate heat transfer system.

3.3. Convergence study for the steady-state numerical solutions

For a steady-state numerical simulation, a solution can be deemed converged by observing the evolution of the following quantities:

– The residual values

– The domain imbalances

– Some global quantities of interest

For an iterative numerical simulation, the residual values quantifies the local variance of a conserved variable in the control volume. Therefore, the residual values of a simulation represents the numerical error in the solution of system of equations and as a consequence, it is important to ensure that their values for each equation is very small (typically less than 10^{-5}). As an example, Figure 7 shows the evolution of residual values with iteration for the steady state solution of the TO problem (Eqn. 2) for the three cases at $\omega = 0.0$, $\omega = 0.5$ and $\omega = 0.99$. Although there are some oscillations in the residual values at higher values of ω due to the increased numerical complexities but more importantly, the values are all below 10^{-5} and hence convergence can be stated.

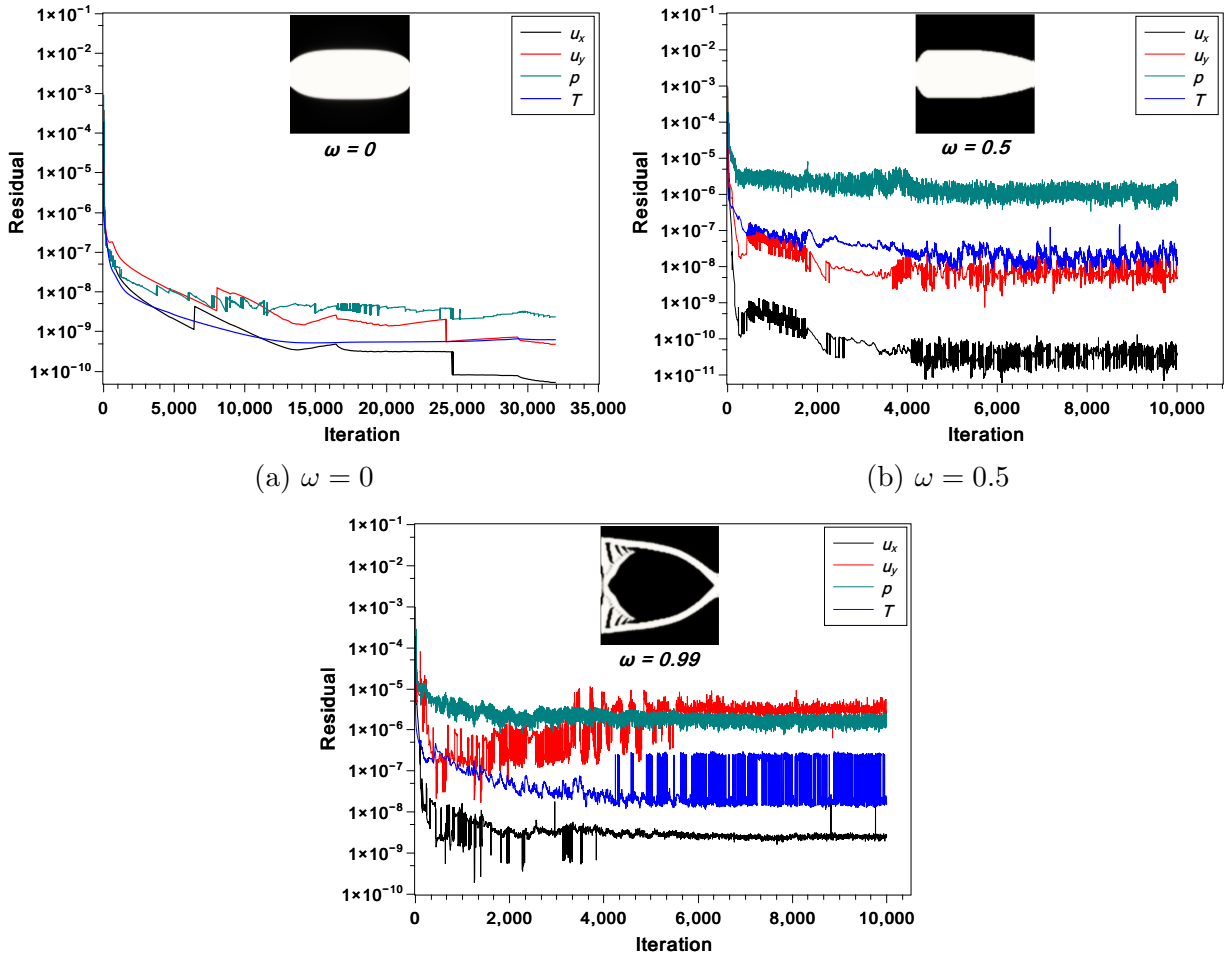

(a) $\omega = 0$

(b) $\omega = 0.5$

(c) $\omega = 0.99$

Figure 7: Residual values for optimal designs obtained from: a) $\omega = 0$, b) $\omega = 0.5$ and c) $\omega = 0.99$.

Secondly, to quantify domain imbalances and to ensure mass conservation in the system, net mass flow rate imbalance is evaluated in the system. Figure 8 presents the difference of

mass flow rate between inlet and outlet (in $kg\ s^{-1}$) as a function of ω (evaluated here for the nine optimal designs in fig. 3 and for $\omega = 1$). It can be seen that the net mass flow rate imbalances are very small of the order of 10^{-15}. Moreover, as the influence of fluid objective function J_f decreases the mass flux imbalance increases marginally to reach its maximum for the optimal design with $\omega = 1$, however, still under the acceptable limits to be deemed mass conserved.

On the contrary, the studies in literature that reported broken flow paths on higher influence of thermal objective function [40][41], may be did not thoroughly respect the mass conservation in the domain. In other words, may be those topology optimization formulation failed to respect the continuity equation equality constraint (Eqn. 2b) during the optimization process.

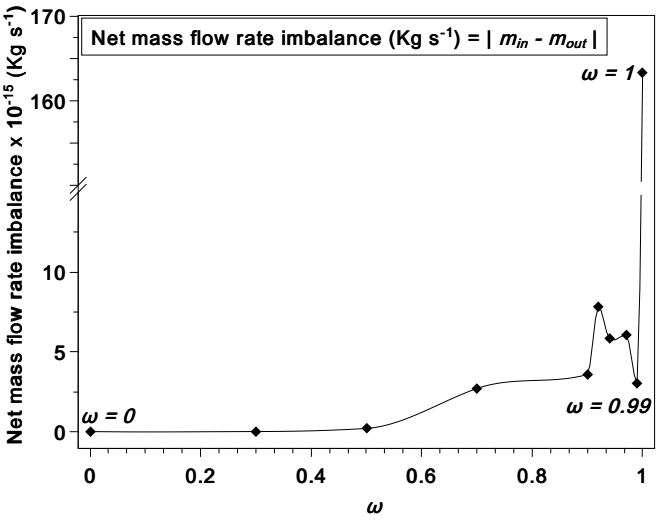

Figure 8: Net mass flow rate imbalances between inlet and outlet of the steady state solution for different optimal designs.

Another criterion to analyze convergence in density based TO is to ensure exact zero velocity values in the solid material for the final design. In the momentum equation (2c), the inverse permeability α is controlled by the design variable η to distinguish the flow in solid and fluid materials which is updated iteratively via the interpolation function (4a). Nevertheless, at a steady state converged solution, the flow motion in solid regions is expected to reach zero velocities. As an example, consider the optimal design obtained at $\omega = 0.99$, where velocity profile is plotted with η values at a randomly selected cross-section ($\tilde{x} = 0.5$) in the domain (Fig. 9). It can be clearly observed that exact zero values are attained in the solid (dark color) regions which testifies convergence at the steady state.

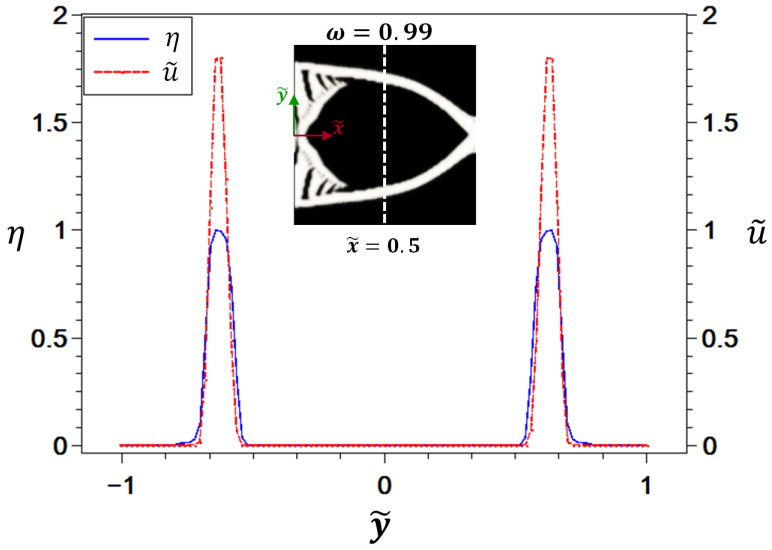

Figure 9: Variation of $\tilde{u}$ with η for the optimal design obtained with $\omega = 0.99$.

Finally, the values of the two objective functions (J_f and J_{th}: evaluated at the domain boundary Γ) itself can be considered as the quantities of interest for the current numerical problem. Additionally, the maximum allowed volume fraction of fluid material ϕ_{max} is also used as a criterion to assure convergence of the numerical TO problem. As an example, Figure 10 shows the convergence history for the TO problem solved iteratively at $\omega = 0.5$ and $\omega = 0.99$.

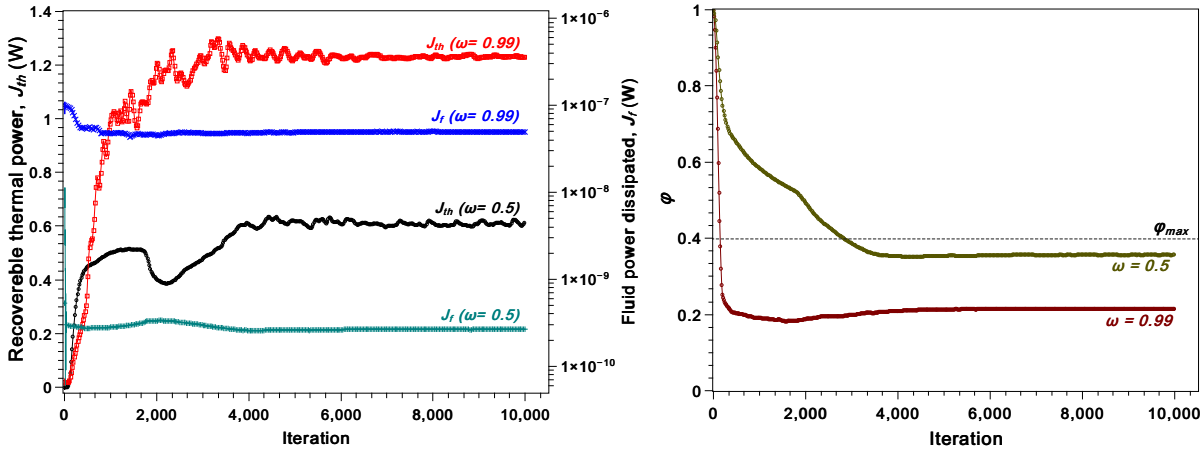

(a) Quantities of interest: J_{th} and J_f

(b) Evolution of ϕ with iteration

Figure 10: Convergence history of the TO problem for the optimal design obtained by $\omega = 0.5$ and $\omega = 0.99$.

3.4. Quantifying the performance of the objective functions

In section 3.1, several designs were presented as an outcome of the multi-objective optimization process. This section attempts to further deepen the understanding of obtained optimal structure by first introducing another performance criteria based on pressure drop

in the fluid channel and then later carrying out an in-depth local analysis at the outlet boundary.

3.4.1. Friction factor (f_d) as the fluid performance criterion

The fluid objective function aims at minimizing the power dissipated by the fluid through the domain and is evaluated from the total pressure losses through the domain boundaries Γ as presented in Eqn. 5. An important criterion from the literature that can be directly associated to pressure drop is the friction factor f_d [61] defined as the following:

$$f_d = \frac{\Delta P}{\frac{1}{2}(l/d)\rho {U_m}^2} \tag{20}$$

where ΔP (in Pa) is the pressure difference between the inlet and outlet boundaries, l (in m) the length of the pipe, d (in m) the hydraulic diameter of the pipe, ρ (in $kg\ m^{-3}$) the density of the fluid and U_m (in $m\ s^{-1}$) is the flow velocity averaged over the cross-sectional area of the pipe outlet. Using equation 20, the friction factor is calculated and shown in Fig. 11 for the different optimal designs presented in Fig. 3. The behavior of the friction factor in the optimal fluid channels is in agreement with that of the fluid objective function J_f. Predictably, the friction factor is of minimum value at $\omega = 0$ and increases rapidly versus increased ω values mainly due to the high pressure drop values between the inlet and outlet. This is due to more priority given in F to maximize J_{th} rather than minimizing J_f. Only at $\omega = 1$, where the fluid path is very complex, the friction factor reaches extremely high values (but still of finite value). The above friction factor (f_d) relation, being more comprehensible as compared to J_f (Eqn. 5) in terms of pressure drop values, gives the user a better insight into the performance of the optimal designs obtained.

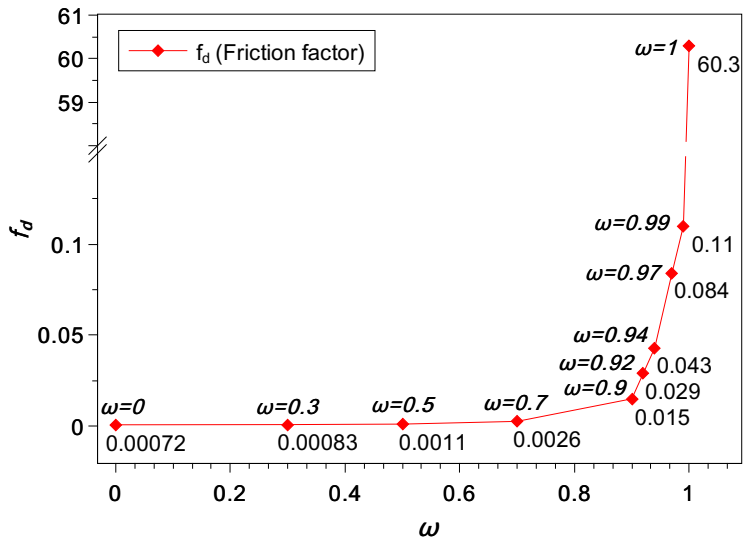

Figure 11: Friction factor (f_d) values for different optimal designs.

3.4.2. Local analysis of the thermal objective J_{th} at the outlet boundary Γ_{out}

The thermal objective function presented in Eqn. (6) computed at the domain total boundary Γ can be detailed as the following:

$$J_{th}(\boldsymbol{u}, T) = \rho C_p \Big[\underbrace{\int_{\Gamma_{\text{in}}} T\boldsymbol{u}\cdot\boldsymbol{n}\, d\Gamma_{\text{in}}}_{\text{constant}} + \underbrace{\int_{\Gamma_{\text{ad}}} T\boldsymbol{u}\cdot\boldsymbol{n}\, d\Gamma_{\text{ad}}}_{=0} + \underbrace{\int_{\Gamma_{\text{w}}} T\boldsymbol{u}\cdot\boldsymbol{n}\, d\Gamma_{\text{w}}}_{=0} + \int_{\Gamma_{\text{out}}} T\boldsymbol{u}\cdot\boldsymbol{n}\, d\Gamma_{\text{out}} \Big] \tag{21}$$

The first term in the above equation remains constant versus iterations because the temperature and velocity profiles are imposed initially at the inlet boundary Γ_{in} (see Fig. 1). The next two terms becomes equal to zero by the virtue of the fact that no-slip velocity boundary condition ($\boldsymbol{u}\cdot\boldsymbol{n} = 0$) was imposed initially at the walls Γ_{ad} and Γ_{w}. Hence, the only term left to optimize (maximize) for the present problem is the fourth term at the outlet Γ_{out} to the right hand side of Eqn. (21). This term is made of two unknown field variables: the temperature and the dot product of the velocity vector and the unit vector normal to the boundary surface at the outlet. Hence, for a more deep analysis of the optimal designs presented in Fig. 3, the normalized temperature and normalized velocity magnitude profiles are plotted at the outlet boundary as shown in Fig. 12 (a) and (b), respectively.

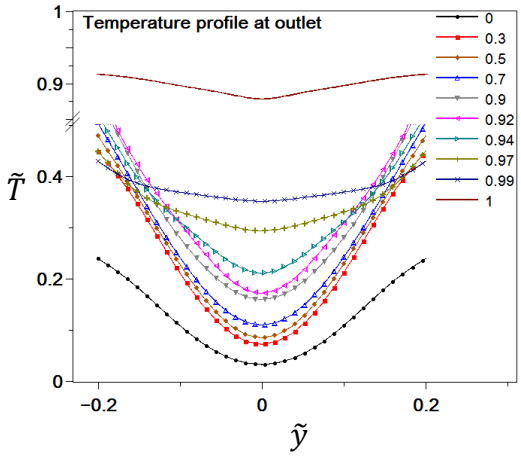

(a) Normalized temperature profiles

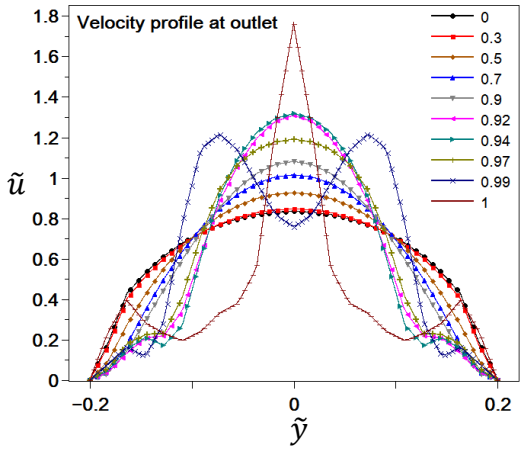

(b) Normalized velocity profiles

Figure 12: a) Normalized temperature and b) Normalized velocity magnitude profiles at the outlet boundary Γ_{out}.

It can be seen from figure 12 that the temperature values at the outlet for the optimal designs at $\omega = 0.3,\ 0.5$ and 0.7 are very close because the TO process here is predominantly trying to maximize the velocity at the outlet by changing the shape of the straight fluid channel (converging it or making it narrower). For the optimal designs from $\omega = 0.9$ onwards, there is a significant increase of both temperature and velocity values at the outlet. Now the TO process can be seen as working at its full potential in order to exploit both the contributing factors in the objective function.

On the contrary, Marck et al.[40] used a constant parabolic velocity outlet condition (same value as at the inlet) for the boundary Γ_{out}. Consequently, the only variable left in the

objective function J_{th} which the TO process could exploit (maximize) was the temperature at the outlet. Knowingly or unknowingly, the choice of inappropriate velocity BC at the outlet restricted the performance of their TO numerical tool to a single variable. As a result, the authors observed splitting of the fluid channel from a very early stage as the only alternative for the TO process was to heat up the fluid by moving it closer to the walls. Additionally, in contrast to the present study, the authors did not observe any fluid channel designs that aimed at increasing the velocity of the fluid (for example, converging or narrowing fluid channels).

3.5. Order of magnitude analysis of the thermal objective function

To justify the order of magnitude of recoverable thermal power values obtained in the present study, the following section aims to approximate analytically the values of J_{th} at the domain boundary on one of the optimal designs presented in Fig. 3. For the current problem, the thermal objective function is evaluated on the domain boundaries Γ as described by Eqn. 21. Following the analysis in the previous section, the equation can be re-written here as follows:

$$J_{th}(\boldsymbol{u}, T) = \rho C_p \left[\Big(\int_{\Gamma_{\text{in}}} T\boldsymbol{u} \cdot \boldsymbol{n} \; d\Gamma_{\text{in}} \Big) + \Big(\int_{\Gamma_{\text{out}}} T\boldsymbol{u} \cdot \boldsymbol{n} \; d\Gamma_{\text{out}} \Big) \right] \tag{22}$$

Thus, the computed value of J_{th} has contribution only from the inlet and the outlet boundary. As an example, the optimal design for $\omega = 0.9$ (see Fig. 3(e)) is considered for the current analysis. Now, if it is assumed that the velocity vector ($\boldsymbol{u}$) and the normal vector to the surface at inlet and outlet ($\boldsymbol{u}$) are exactly parallel to each other, then the above equation can be simplified as follows:

$$J_{th}\Big|_{approx} = \rho C_p \Big[\underbrace{- \int_{\Gamma_{\text{in}}} T u_x \; d\Gamma_{\text{in}}}_{\text{I}} + \underbrace{\int_{\Gamma_{\text{out}}} T u_x \; d\Gamma_{\text{out}}}_{\text{II}} \Big] \tag{23}$$

Note that the negative sign in the above equation appears due to the opposite signs of normal vector to the surface at inlet and outlet boundary in OpenFOAM software package. The two integral terms in equation 23 can be easily evaluated from Fig. 13 as the area under the curve for the the function Tu_x at inlet and outlet, respectively. Additionally, for the current study $\rho = 1000 \; kg \; m^{-3}$ and $C_p = 5000 \; Jkg^{-1}K^{-1}$. Hence, the value of thermal objective function for the optimal design with $\omega = 0.9$ can be approximated as:

$$J_{th}\Big|_{approx} = 1000 \times 5000 \Big[- (1.822 \times 10^{-5}) + (1.837 \times 10^{-5}) \Big] = 0.75 \; W \tag{24}$$

The approximate value of thermal objective function obtained by above analysis is very close to the numerical value of 0.76 W reported by the TO method but more importantly this analysis justifies the order of magnitude of the thermal objective function obtained in the present study.

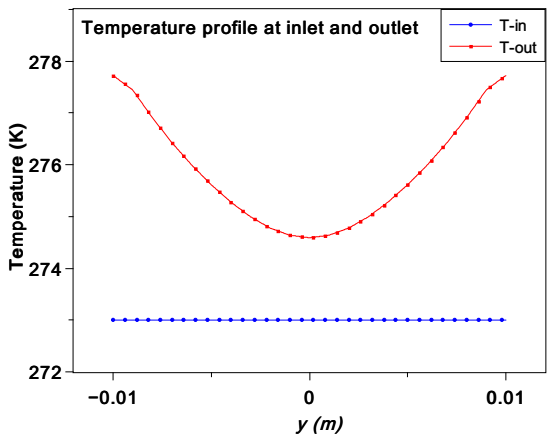

(a) T profile at inlet (blue) and outlet (red).

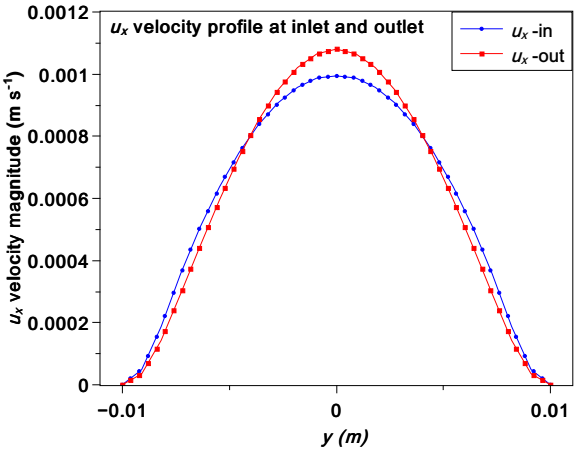

(b) u_x profile at inlet (blue) and outlet (red).

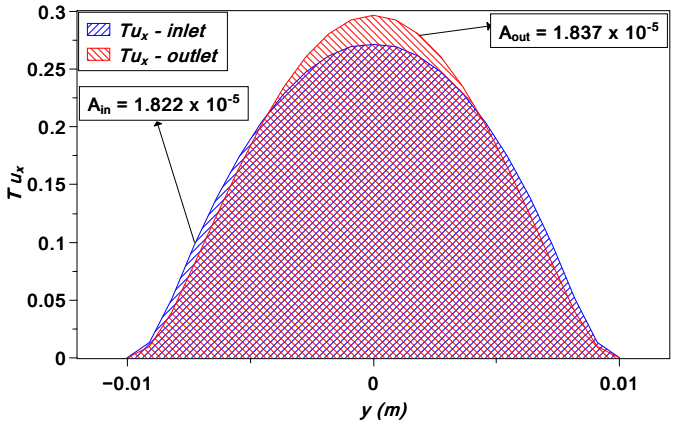

(c) Area under the curve for product (Tu_x) at inlet (blue) and outlet (red).

Figure 13: Analytical evaluation of the thermal objective function J_{th} at inlet and outlet boundaries for the optimal design obtained with $\omega = 0.9$: a) Temperature profile at inlet and outlet, b) u_x velocity profile at inlet and outlet, and c) Area under the curve for the product Tu_x.

3.6. Influence of variation of physical and numerical parameters on the optimal designs for CHT systems

This section demonstrates the effect of variation of some physical and numerical parameters on the final optimal topology of CHT systems. The objective here is to test the ability of developed multi-objective TO numerical solver in producing physically logical structures on varying some important parameters in the optimization problem. For the sake of simplicity, the results in this section are presented only for two values of ω.

3.6.1. Fluid as the higher thermal diffusivity material

All the results obtained in section 3.1 considered solid as the higher thermal diffusivity material in the domain such that $\gamma = D_s/D_f = 10$. Therefore, as the first parameter, the optimization problem described in section 2 is re-evaluated with the reversed thermal diffusivity ratio such that the fluid material now has the higher thermal diffusivity in the domain i.e. $\gamma = D_s/D_f = 0.1$ and all other parameters unchanged.

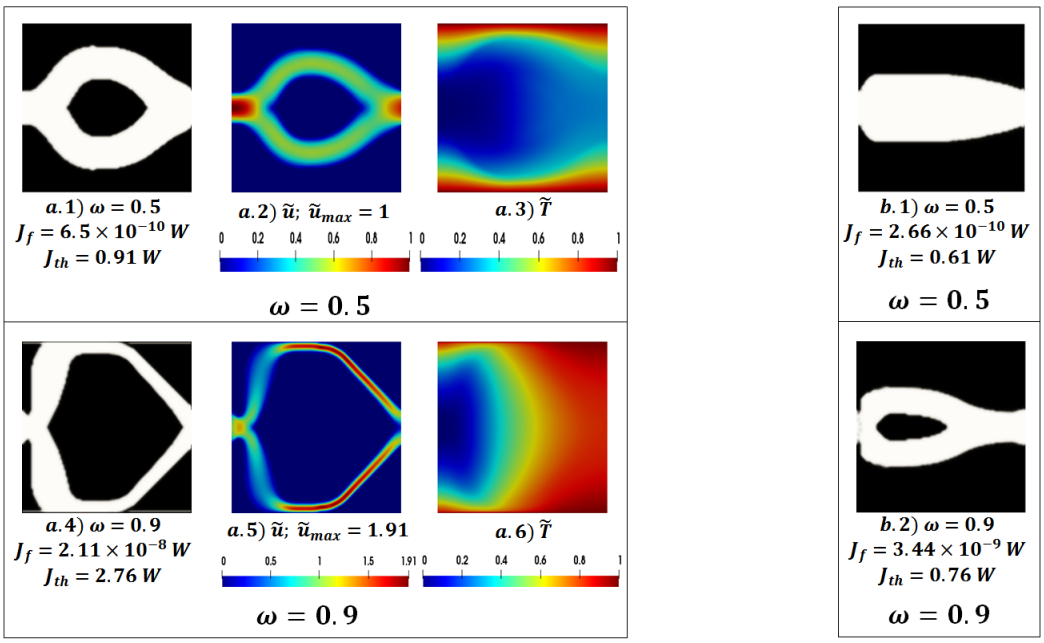

Optimal designs obtained when fluid has higher thermal diffusivity:
$\gamma = D_s/D_f = 0.1$;
$\Delta T = 10K$ & $Re = 3$.

(a) Fluid with the higher thermal diffusivity

Original optimal designs from Fig. 2:
$\gamma = D_s/D_f = 10$;
$\Delta T = 10K$ & $Re = 3$.

(b) Solid with the higher thermal diffusivity

Figure 14: Optimal designs obtained for $\omega = 0.5$ and $\omega = 0.9$ with: a) Fluid as the higher thermal diffusivity material and b) Solid as the higher thermal diffusivity material in the domain.

Figure 14 (a) shows the optimal design obtained for $\omega = 0.5$ and $\omega = 0.9$ with fluid as the higher thermal diffusivity material . In contrast to the previous results (Figure 14 (b)), the fluid channel is already split into two upper and lower fluid paths at $\omega = 0.5$ and moreover these fluid paths move very close to the heated walls at $\omega = 0.9$. This behavior of the optimal fluid channels design can be attributed to the inability of the solid material to conduct more heat to the passing fluid in the current problem. Consequently, on increasing ω, the higher thermal diffusive (or conductive) fluid material attempts to position itself closer to the heat source (the heated walls) in order to extract maximum thermal power from the system. As for the similarities, the fluid channels continue to become narrower on increasing ω in order to increase velocity of the fluid at the outlet which eventually increases the thermal objective function.

3.6.2. Variation of maximum temperature gradient in the system

The problem description in section 2 considered a temperature difference of 10 Kelvin between the cold incoming fluid (T_{in}) and the top and bottom heated walls (T_w). Therefore, the next parameter involves varying the thermal boundary conditions in the domain by changing the maximum temperature gradient in the system. Consequently, the original problem in section 2 is re-evaluated with the modified thermal boundary conditions for the three different cases as follow:

– Cold fluid and hot walls: $\Delta T = (T_w - T_{in}) = 313\ K - 273\ K = 40\ K$

– Cold fluid and hot walls: $\Delta T = (T_w - T_{in}) = 353\ K - 273\ K = 80\ K$

– Hot fluid and cold walls: $\Delta T = (T_w - T_{in}) = 273\ K - 283\ K = -10\ K$

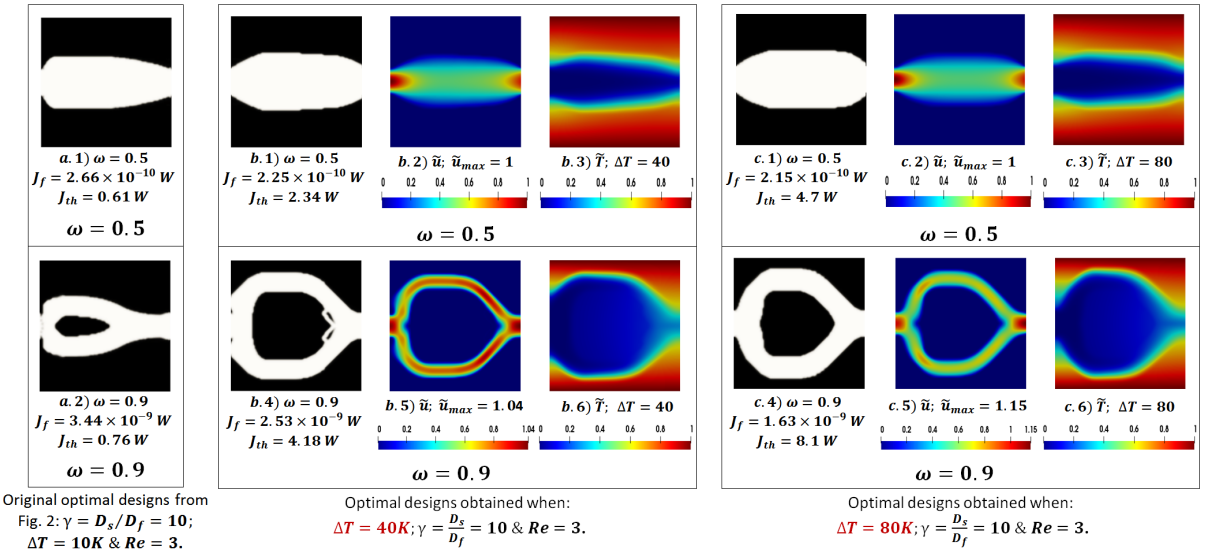

(a) $\Delta T = 10\ K$ (b) $\Delta T = 40\ K$ (c) $\Delta T = 80\ K$

Figure 15: Optimal designs for modified thermal boundary conditions: The thermal diffusivity ratio between solid and fluid maintained as $\gamma = D_s/D_f = 10$ with Cold incoming fluid and hot walls for a) $\Delta T = 10\ K$, b) $\Delta T = 40\ K$ and c) $\Delta T = 80\ K$.

ΔT in (Kelvin)	J_f in (Watts)	J_{th} in (Watts)
$\omega = 0.5$		
10	2.66×10^{-10}	0.61
40	2.25×10^{-10}	2.34
80	2.15×10^{-10}	4.7
$\omega = 0.9$		
10	3.44×10^{-9}	0.76
40	2.53×10^{-9}	4.18
80	1.63×10^{-9}	8.1

Table 1: Objective function values for the optimal designs with $\omega = 0.5$ and $\omega = 0.9$ for the three values of maximum temperature gradient in the domain (ΔT = 10 K, 40 K and 80 K with cold incoming fluid and heated walls).

On comparison with the previous results obtained in with ΔT =10 K (Fig. 15 (a)), Figure 15(b) and (c) show the optimal designs obtained for cold incoming fluid and heated

walls boundary conditions with ΔT =40 K and ΔT =80 K, respectively. Table 1 summarizes the objective function values for the optimal designs with $\omega = 0.5$ and $\omega = 0.9$ for the three values of maximum temperature gradient in the domain (ΔT = 10 K, 40 K and 80 K with cold incoming fluid and heated walls).

The pattern of optimal design evolution with ω remains similar for the three cases whenever the incoming fluid is cold and the top and bottom walls are hot i.e. ($T_w > T_{in}$). Additionally, as expected, the value of thermal objective function significantly increases with increasing value of ΔT because of the possibility of recovering more heat from the domain.

Figure 16 shows the optimal design obtained when the incoming fluid is hot and the top and bottom walls are cold ($T_{in} > T_w$) with $\Delta T = T_w - T_{in} = -10\ K$. Interestingly, in contrast to the previous results, the fluid channel between inlet and outlet attempts to move away as far as possible from the cold walls in order to prevent the heat loss from the passing fluid, on increasing the value of ω. Such optimal designs clearly demonstrate the ability of the developed multi-objective TO numerical solver in producing physically logical designs by appropriately responding to any critical changes in the problem description.

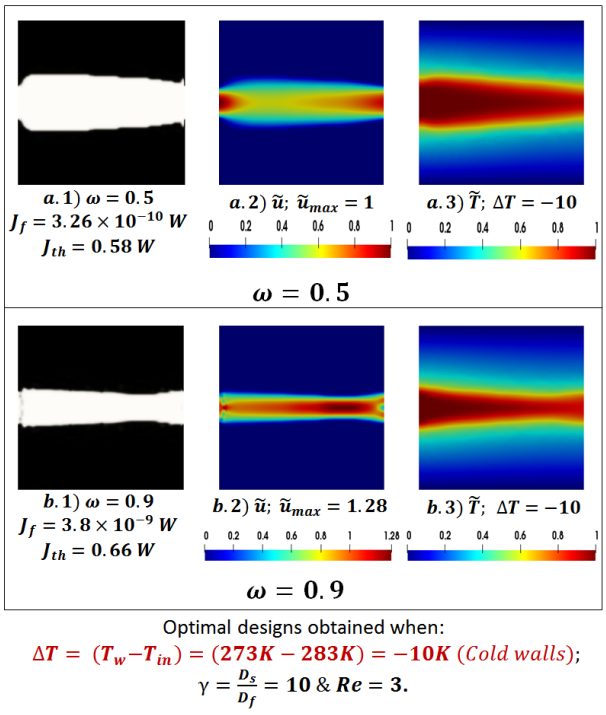

Figure 16: Optimal designs for modified thermal boundary conditions: The thermal diffusivity ratio between solid and fluid maintained as $\gamma = D_s/D_f = 10$ with Hot incoming fluid and cold walls for $\Delta T = -10\ K$

3.6.3. Variation of the Reynolds number

The original problem in section 2 (which considered a Reynolds number of $Re = 3$) is solved again for $Re = 10$ and $Re = 100$ by augmenting the inlet fluid velocity. Figure 17 present the optimal designs for $Re = 10$ and $Re = 100$, respectively compared with the previous results obtained for $Re = 3$ for the two values of ω. Additionally, Table 2 summarizes the objective function values for the optimal designs with $\omega = 0.5$ and $\omega = 0.9$ for the three

different values of Reynolds number of the incoming fluid. Evidently, there is a significant increase in fluid objective function J_f as the Re increases due to the higher fluid velocities in system. Another important observation is the moderate increase in thermal objective function J_{th} on increasing Re even when the thermal boundary condition are same for the three cases. This comes as a direct consequence of the contribution of velocity term in the thermal objective function. Finally, it can be clearly observed from Table 1 and 2 that the objective function J_f is more sensitive to inertial influence of increasing Re whereas the objective function J_{th} is more sensitive to increase of ΔT in the domain.

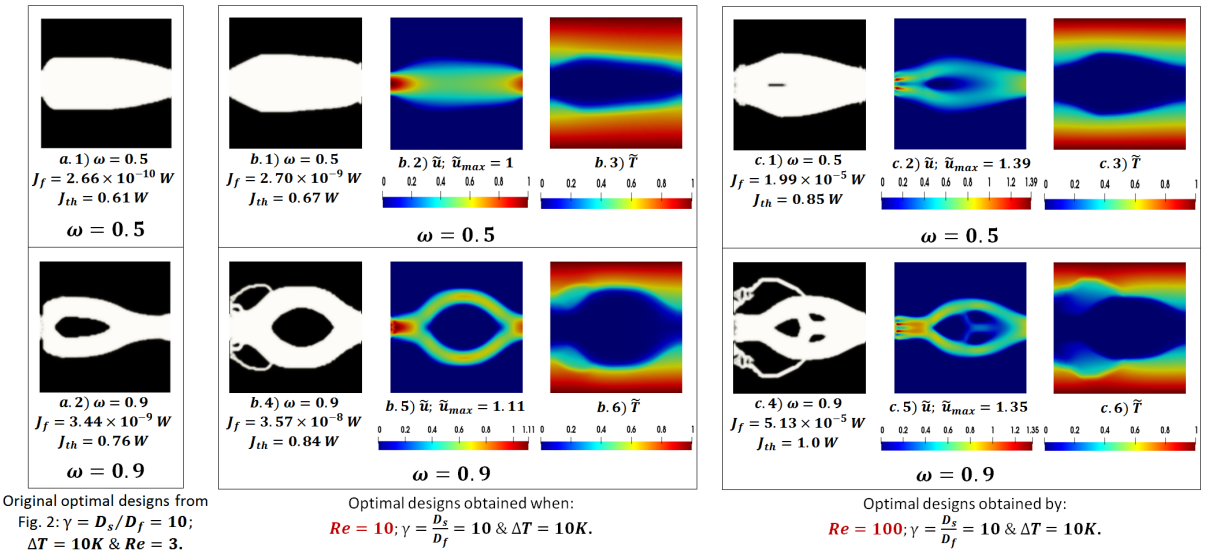

(a) $Re = 3$ (b) $Re = 10$ (c) $Re = 100$

Figure 17: Optimal designs obtained with the thermal diffusivity ratio between solid and fluid maintained as $\gamma = D_s/D_f = 10$ and varying the Reynolds number as: a) $Re = 3$, b) $Re = 10$ and c) $Re = 100$.

Re	J_f in (Watts)	J_{th} in (Watts)
$\omega = 0.5$		
3	2.66×10^{-10}	0.61
10	2.70×10^{-9}	0.67
100	1.99×10^{-5}	0.85
$\omega = 0.9$		
3	3.44×10^{-9}	0.76
10	3.57×10^{-8}	0.84
100	5.13×10^{-5}	1.0

Table 2: Objective function values for the optimal designs with $\omega = 0.5$ and $\omega = 0.9$ for the three different values of Reynolds number of the incoming fluid: Re =3, Re = 10 and Re = 100.

3.6.4. Influence of spatial discretization

Next, the influence of spatial discretization of the computational domain on the topology optimized designs is analysed. The original conjugate heat transfer optimization problem described in section 2 is solved on five different meshes (consisting of 60×60, 80×80, 100×100, 120×120 and 140×140 square-cell design elements, respectively) and the two objective function values are monitored on the converged solution. Subsequently, the relative percentage error is also evaluated for each case. Figure 18 presents the corresponding optimal designs and the associated objective function values (J_f and J_{th}) for two different values of ω: $\omega = 0.5$ and $\omega = 0.94$. For each value of ω, the design with the best (lowest) fluid objective function values is highlighted with a blue box and the one with best (highest) thermal objective function value is highlighted with red box. Additionally, Fig. 19 and 20 plots the variation of the fluid objective function (J_f) and the thermal objective function (J_{th}) along with the associated relative percentage error with increasing mesh size for the two values of ω, respectively.

As a first observation, it can can be seen that the final optimal designs share similar design forms, however, with better and clearer description of fluid channel boundaries with increasing mesh size. Moreover, the plots in Fig. 19 and 20 depicts the general trend of obtaining better objective function values with higher mesh size. On further observation, it can be seen that very close objective function values are obtained with the last two meshes which use 120×120 and 140×140 design elements, respectively. Hence, it can be said that mesh independent designs for the current problem can be obtained by using a mesh resolution of 120×120 cells.

ω	60×60 Cells	80×80 Cells	100×100 Cells	120×120 Cells	140×140 Cells
0.5					
J_f(W)	5.21×10^{-10}	2.345×10^{-10}	2.66×10^{-10}	2.34×10^{-10}	2.20×10^{-10}
$J_{th}(W)$	0.52	0.59	0.61	0.63	0.62
0.94					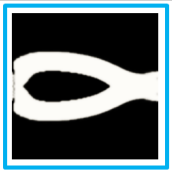
J_f	1.20×10^{-8}	1.04×10^{-8}	9.15×10^{-9}	7.81×10^{-9}	7.2×10^{-9}
J_{th}	0.73	0.85	0.86	0.90	0.87

Figure 18: Optimal designs for $\omega = 0.5$ and $\omega = 0.94$ obtained with five different mesh sizes: 60×60, 80×80, 100×100, 120×120 and 140×140 square-cell designs elements, respectively.

Generally, density-based TO approach is believed to suffer from mesh-dependence problem i.e., the problem of not obtaining qualitatively the same solution for different spatial

discretization also reffered as obtaining *non-unique solutions* or several optima. This problem is acknowledged by several authors who dealt with heat conduction or structural TO problems [17, 58]. However, the results in Fig. 18 clearly show that the current topology optimization model does not suffer from mesh-dependency numerical instability when using a Cartesian grid with orthogonal square elements.

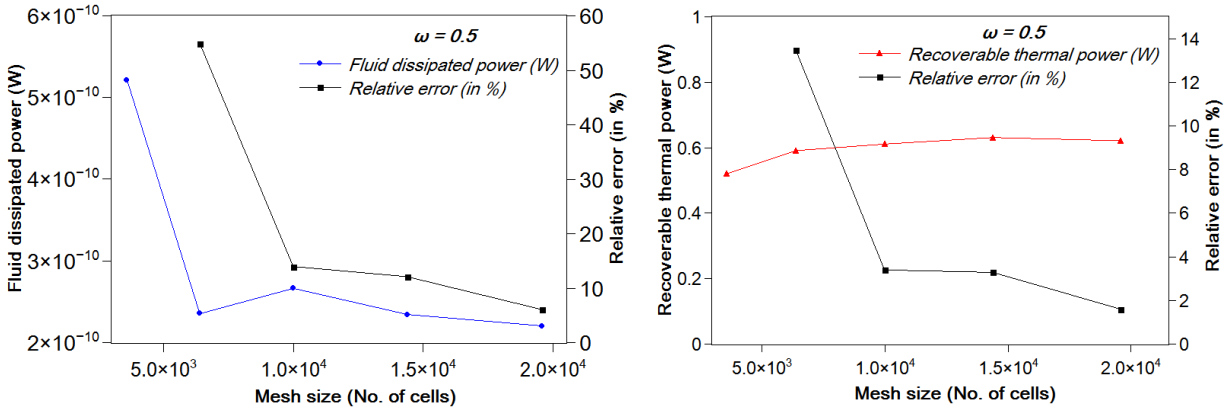

(a) Fluid dissipated power. (b) Recoverable thermal power.

Figure 19: Variation of objective function values and the associated relative percentage error with increasing mesh size for the optimal design obtained with $\omega = 0.5$.

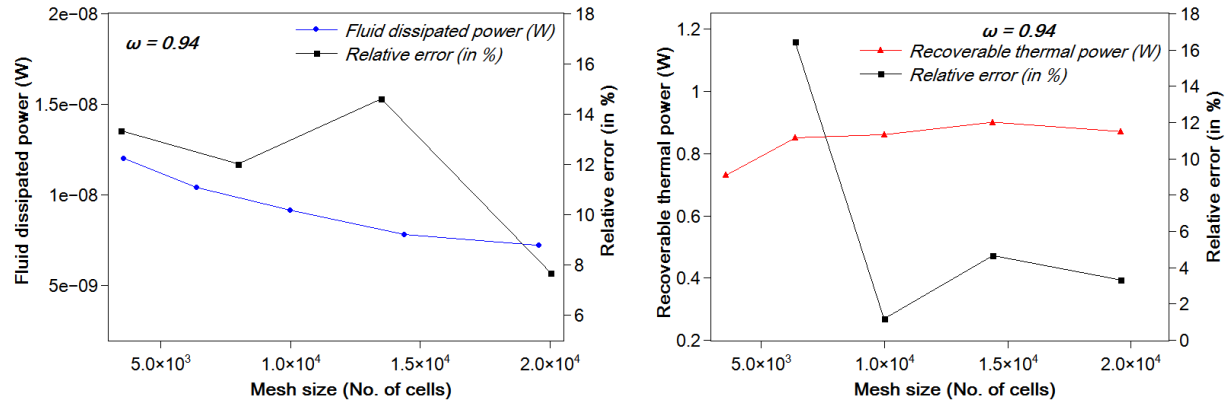

(a) Fluid dissipated power. (b) Recoverable thermal power.

Figure 20: Variation of objective function values and corresponding relative percentage error with increasing mesh size for the optimal design obtained with $\omega = 0.94$.

3.6.5. Comparison of topology optimization approaches

In this section, we analyze the results obtained by two different topology optimization approaches for the same design problem by comparing their optimal designs in terms of objective function values. The present TO numerical platform is based on the Finite Volume Method (FVM) as the discretization technique coupled to a density approach for material distribution in the domain, RAMP-type interpolation functions in this case. It is applied to a recent conjugate heat transfer topology optimization problem taken from the literature by [44] where the authors solved the optimization problem using the Lattice Boltzmann

Method (LBM) as discretization technique coupled to a Level Set Method (LSM) for material boundary representation in the domain.

The FVM is based on discretizing macroscopic continuum equations while the LBM deals with microscopic models and mesoscopic kinetic equations where the displacement and collision of particles are solved via the Boltzmann equation [44][62]. In addition to this, both approaches use gradient-based local optimization algorithms complemented by the continuous adjoint method for sensitivity analysis. Both the optimization approaches try to maximize the same thermal objective function, however Dugast et al. [44] refers it as the heat exchange efficiency characterized by the amount of heat evacuated from the fluid. On the other hand, in the he present study it referred as the thermal power recovered by the fluid. Essentially, both the objective function are the same as they aim to maximize the term $T(\mathbf{u} \cdot \mathbf{n})$ at the outlet boundary Γ_{out}.

The 2D design domain and the boundary conditions of the optimization problem by [44] are shown in Fig. 21. The gray and white zones near the boundary are fixed solid and fluid parts, respectively. The rest of the geometry is very similar to the original problem description of the fluid channel with an inlet and an outlet as shown in Fig. 1. The length of the heated segment at the bottom wall ($0.04\ m$) is longer that the top wall ($0.02\ m$) in order to introduce an asymmetric effect.

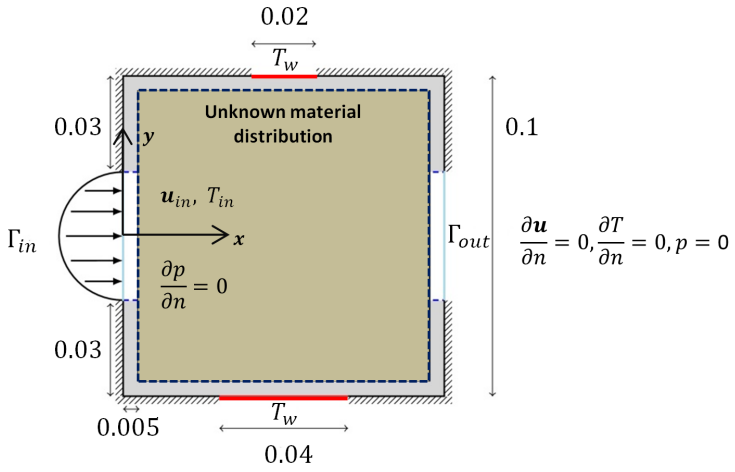

Figure 21: Initial configuration of the optimization problem (adapted from Dugast et al.[44]): All dimensions are in m.

The physical and numerical parameters for the above optimization problem based on the works by Dugast et al. [44] are as the following:

- fluid material: water (constant physical properties at $T = 45°$)
- solid material: constant thermal properties of water
- spatial discretization of the domain: 100×100 elements
- maximum allowed porosity: $\phi_{max} = 0.5$

– Reynolds number at inlet: $Re = 25$

– inlet fluid temperature: $20°C$

– heated segment temperature at top and bottom walls: $100°C$.

– initialization: full fluid

In order to ensure consistency and better compare the performance of the optimal fluid channel designs, the two optimal structures obtained from the present OpenFOAM TO numerical platform and from that by Dugast et al. [44], respectively for the same optimization problem are extracted and then simulated in STAR-CCM+®commercial CFD software package using identical grid settings and numerical schemes to get the objective function values. Figure 22 shows the two optimal designs and the associated velocity magnitude, temperature and pressure contours obtained from CFD simulations. Table 3 gives the objective function values and the pressure drop for two optimal designs.

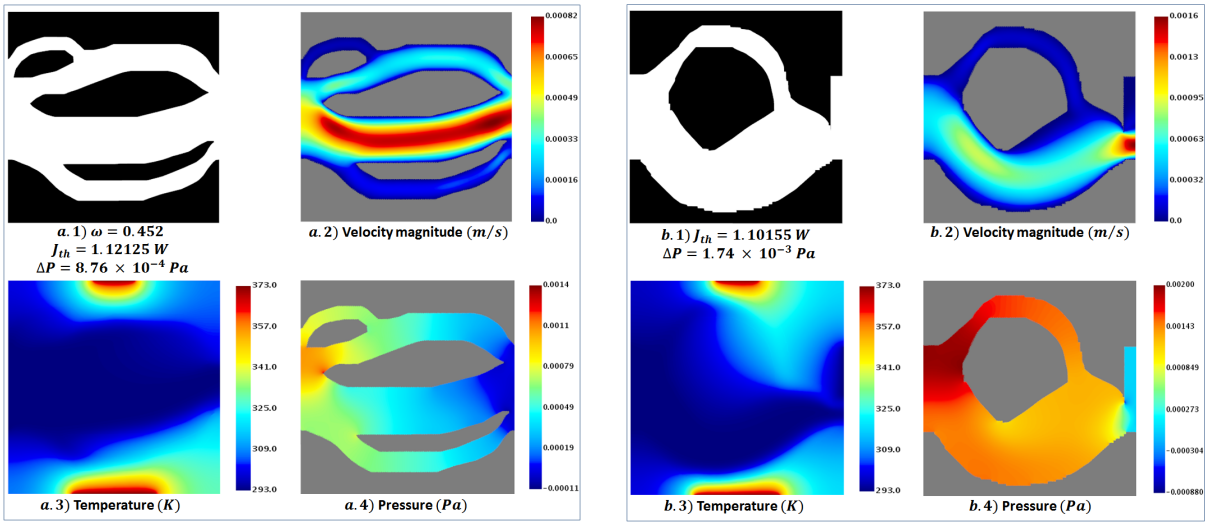

(a) Optimal design obtained in the present study. (b) Optimal design obtained by Dugast et al. [44].

Figure 22: Optimal designs obtained with : a) FVM discretization with density approach TO (present study) and b) LBM coupled to LSM for TO (Dugast et al. [44]).

Discretization method	J_{th} in (Watts)	ΔP in (Pa)
FVM (present study)	1.12125	8.76×10^{-4}
LBM (Dugast et al.)	1.10155	1.74×10^{-3}

Table 3: Objective function and pressure drop values for the optimal designs achieved from FVM and LBM dicretization methods.

Comparison the two structures, it can be observed that the objective function value (thermal power) of the optimal design obtained by the present FVM-based TO platform

is marginally higher than that obtained by Dugast et al. [44] but more importantly with around 50% less pressure drop as compared to the latter. This means that the present FVM-based TO platform coupled with the density approach produced better optimal design than that produced by [44] which is LBM-based TO platform coupled to level-sets for boundary representation. The high pressure drop values for the LBM optimal design can be attributed to the partial obstruction of the flow near the outlet (see Fig. 22b) which the LBM-based optimization approach created on purpose in order to increase the fluid velocity at the outlet which has a direct contribution in the thermal objective function. On the other hand, the bi-objective function strategy (with $\omega = 0.452$), the TO numerical platform in the present study was able to achieve similar thermal objective function values but with significantly reduced pressure drop value in the system with no obstruction at the outlet. This comparison clearly shows the advantage of using a bi-objective optimization approach particularly in topology optimization of conjugate heat transfer systems.

As for the similarities between the two designs, one can observe that both designs are asymmetric due to the asymmetric nature of the problem. Additionally, in both designs, the bulk of the fluid mass is pushed towards the bottom heated element as a direct consequence of its larger dimension compared to the top heated element. It should be noted that the thermal conductivity of the fluid and solid material are the same for this problem in Fig 21 which was taken as the thermal conductivity of water.

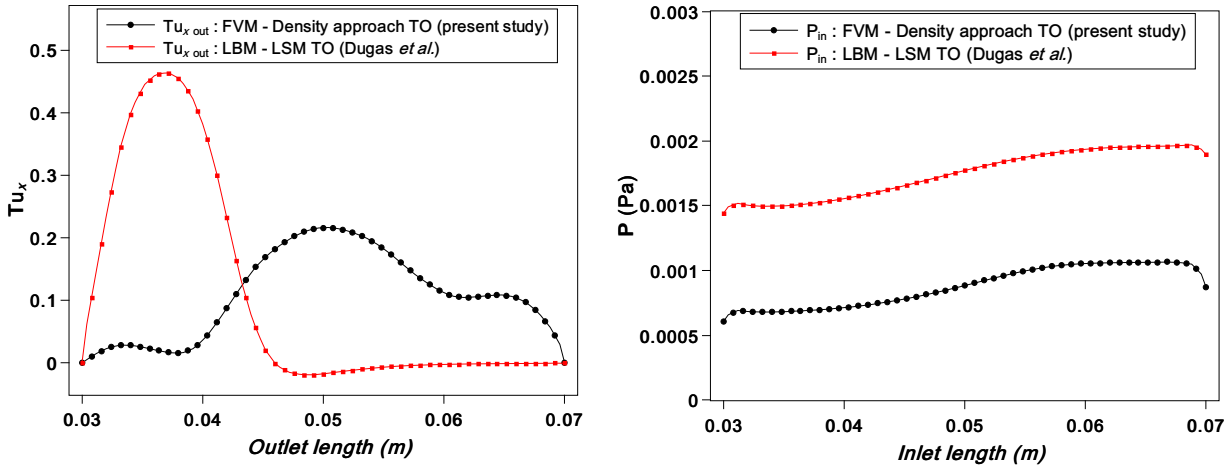

(a) Tu_x profile at outlet.

(b) Pressure profile at inlet.

Figure 23: Local analysis of the results at the domain boundary for the two designs: a) Comparison of the product Tu_x at outlet and b) Comparison of pressure profile at inlet.

Since the thermal objective function, which the optimization algorithm aims to maximize, is a product of temperature (T) and a horizontal component of velocity (u_x) at the outlet boundary, Fig. 23 represents a good methodology for deeper analysis. It illustrates the Tu_x profile at outlet and compares the pressure profile at inlet for the two obtained designs. Although there is a major increase of the product Tu_x near the bottom part at the outlet boundary for the LBM-based design, the overall average is slightly less than that of the FVM-based design due to the null fluid velocity at rest at the outlet boundary. This local analysis of results at the inlet and outlet boundaries justifies well the objective function and

pressure drop values reported in Table 3.

4. Conclusion

Topology optimization of conjugate heat transfer systems using a challenging coupled bi-objective function, for heat transfer enhancement and pressure drop reduction, has been developed and presented for laminar incompressible flows. The continuous adjoint method has been implemented for gradient computation within a density-based based approach for material distribution. The new topology optimization numerical platform is coupled to an inequality constrained optimization algorithm [56, 31] inside an open source CFD platform which uses the Finite Volume Method as the discretization technique.

The present numerical approach was then applied to an optimization problem from the literature [40] for optimizing a typical fluid channel domain with constant walls temperature different to the one imposed at the domain's inlet. The Pareto set of several optimal designs are computed, presented and analyzed.

It is found that the present developed numerical technique efficiently generates realistic topological optimal designs for conjugate heat transfer systems starting from pressure drop minimization to thermal power maximization based on the value of the weighting function. Notably, there is no fluid blockage, broken paths or other non-physical features observed in the optimal designs even at very high weighting factor of thermal objective function. Additionally, for the first time to our knowledge, an in-depth convergence study presented on the optimal structures confirmed that the developed numerical method respects well the equality (fluid continuity and momentum conservation equations) and inequality (imposed volume fraction of one material) constraints of the topology optimization problem.

A detailed analysis of the obtained optimal designs has been conducted. The friction factor has been computed as alternative performance criterion for pressure drop in the system. The obtained temperature and velocity profiles at the domain's outlet have been analyzed and justified. Moreover, an order of magnitude analysis was performed for the thermal objective function to justify its values obtained in the present study as compared to those obtained by [40].

A parametric study has been performed demonstrating the capability of the developed numerical platform in producing realistic structures (i.e., influence of the Reynolds number, spatial discretization, thermal diffusivity ratio and imposed temperature difference between the wall and the inlet).

Finally, a comparison of two different topology optimization approaches is presented for optimization of conjugate heat transfer systems. In that purpose, a recent CHT TO problem (from the literature [44]) which was solved **via a LBM-based solver coupled to level-sets** for boundary representation is solved again using the current developed TO platform but **via a FVM-based solver coupled to a density approach** for material distribution. Comparisons of results for the thermal power maximization and pressure drop reduction values of the obtained designs emphasized that the present FVM-based TO solver outperformed the LBM-based TO solver of [44] for this CHT TO problem.

Future experimental measurements, on some of the obtained optimal structures, will be conducted soon in order to quantify well the limits of validity of our topology optimization overall approach.

References

[1] W. M. Kays, A. L. London, Compact heat exchangers.

[2] M. P. Bendsøe, N. Kikuchi, Generating optimal topologies in structural design using a homogenization method, Computer methods in applied mechanics and engineering 71 (2) (1988) 197–224.

[3] T. Dbouk, A review about the engineering design of optimal heat transfer systems using topology optimization, Applied Thermal Engineering 112 (2017) 841–854.

[4] M. C. E. Manuel, P. T. Lin, Heat exchanger design with topology optimization, in: Heat Exchangers-Design, Experiment and Simulation, InTech, 2017.

[5] M. P. Bendsøe, Optimal shape design as a material distribution problem, Structural optimization 1 (4) (1989) 193–202.

[6] M. Zhou, G. Rozvany, The coc algorithm, part ii: topological, geometrical and generalized shape optimization, Computer Methods in Applied Mechanics and Engineering 89 (1-3) (1991) 309–336.

[7] H. Mlejnek, Some aspects of the genesis of structures, Structural Optimization 5 (1-2) (1992) 64–69.

[8] G. Allaire, F. Jouve, A.-M. Toader, A level-set method for shape optimization, Comptes Rendus Mathematique 334 (12) (2002) 1125–1130.

[9] M. Y. Wang, X. Wang, D. Guo, A level set method for structural topology optimization, Computer methods in applied mechanics and engineering 192 (1) (2003) 227–246.

[10] K. Yaji, T. Yamada, M. Yoshino, T. Matsumoto, K. Izui, S. Nishiwaki, Topology optimization using the lattice boltzmann method incorporating level set boundary expressions, Journal of Computational Physics 274 (2014) 158 – 181. doi:https://doi.org/10.1016/j.jcp.2014.06.004.
URL http://www.sciencedirect.com/science/article/pii/S0021999114004112

[11] J. Sokolowski, A. Zochowski, On the topological derivative in shape optimization, SIAM journal on control and optimization 37 (4) (1999) 1251–1272.

[12] B. Bourdin, A. Chambolle, Design-dependent loads in topology optimization, ESAIM: Control, Optimisation and Calculus of Variations 9 (2003) 19–48.

[13] Y. M. Xie, G. P. Steven, A simple evolutionary procedure for structural optimization, Computers & structures 49 (5) (1993) 885–896.

[14] O. Sigmund, K. Maute, Topology optimization approaches, Structural and Multidisciplinary Optimization 48 (6) (2013) 1031–1055.

[15] A. Gersborg-Hansen, M. P. Bendsøe, O. Sigmund, Topology optimization of heat conduction problems using the finite volume method, Structural and multidisciplinary optimization 31 (4) (2006) 251–259.

[16] J. Dirker, J. P. Meyer, Topology optimization for an internal heat-conduction cooling scheme in a square domain for high heat flux applications, Journal of Heat Transfer 135 (11) (2013) 111010.

[17] G. Marck, M. Nemer, J.-L. Harion, S. Russeil, D. Bougeard, Topology optimization using the simp method for multiobjective conductive problems, Numerical Heat Transfer, Part B: Fundamentals 61 (6) (2012) 439–470.

[18] F. H. Burger, J. Dirker, J. P. Meyer, Three-dimensional conductive heat transfer topology optimization in a cubic domain for the volume-to-surface problem, International Journal of Heat and Mass Transfer 67 (2013) 214–224.

[19] V. Subramaniam, T. Dbouk, J.-L. Harion, Topology optimization of conductive heat transfer devices: An experimental investigation, Applied Thermal Engineering 131 (2018) 390–411.

[20] T. Borrvall, J. Petersson, Topology optimization of fluids in stokes flow, International journal for numerical methods in fluids 41 (1) (2003) 77–107.

[21] A. Gersborg-Hansen, O. Sigmund, R. B. Haber, Topology optimization of channel flow problems, Structural and Multidisciplinary Optimization 30 (3) (2005) 181–192.

[22] L. H. Olesen, F. Okkels, H. Bruus, A high-level programming-language implementation of topology optimization applied to steady-state navier-stokes flow, arXiv preprint physics/0410086.

[23] C. Othmer, E. de Villiers, H. G. Weller, Implementation of a continuous adjoint for topology optimization of ducted flows, in: 18th AIAA Computational Fluid Dynamics Conference, June, 2007.

[24] C. Othmer, A continuous adjoint formulation for the computation of topological and surface sensitivities of ducted flows, International Journal for Numerical Methods in Fluids 58 (8) (2008) 861–877.

[25] Y. Deng, Z. Liu, P. Zhang, Y. Liu, Y. Wu, Topology optimization of unsteady incompressible navierstokes flows, Journal of Computational Physics 230 (17) (2011) 6688 – 6708. doi:https://doi.org/10.1016/j.jcp.2011.05.004.
URL http://www.sciencedirect.com/science/article/pii/S0021999111003019

[26] L. Yin, G. Ananthasuresh, A novel topology design scheme for the multi-physics problems of electro-thermally actuated compliant micromechanisms, Sensors and Actuators A: Physical 97 (2002) 599–609.

[27] T. E. Bruns, Topology optimization of convection-dominated, steady-state heat transfer problems, International Journal of Heat and Mass Transfer 50 (15-16) (2007) 2859–2873.

[28] S.-H. Ahn, S. Cho, Level set–based topological shape optimization of heat conduction problems considering design-dependent convection boundary, Numerical Heat Transfer, Part B: Fundamentals 58 (5) (2010) 304–322.

[29] A. Iga, S. Nishiwaki, K. Izui, M. Yoshimura, Topology optimization for thermal conductors considering design-dependent effects, including heat conduction and convection, International Journal of Heat and Mass Transfer 52 (11-12) (2009) 2721–2732.

[30] G. H. Yoon, Topological design of heat dissipating structure with forced convective heat transfer, Journal of Mechanical Science and Technology 24 (6) (2010) 1225–1233.

[31] K. Svanberg, The method of moving asymptotesa new method for structural optimization, International journal for numerical methods in engineering 24 (2) (1987) 359–373.

[32] E. M. Dede, Multiphysics topology optimization of heat transfer and fluid flow systems, in: proceedings of the COMSOL Users Conference, 2009.

[33] K. Lee, Topology optimization of convective cooling system designs.

[34] M. Stolpe, K. Svanberg, An alternative interpolation scheme for minimum compliance topology optimization, Structural and Multidisciplinary Optimization 22 (2) (2001) 116–124.

[35] T. Matsumori, T. Kondoh, A. Kawamoto, T. Nomura, Topology optimization for fluid–thermal interaction problems under constant input power, Structural and Multidisciplinary Optimization 47 (4) (2013) 571–581.

[36] P. E. Gill, W. Murray, M. A. Saunders, Snopt: An sqp algorithm for large-scale constrained optimization, SIAM review 47 (1) (2005) 99–131.

[37] E. Kontoleontos, E. Papoutsis-Kiachagias, A. Zymaris, D. Papadimitriou, K. Giannakoglou, Adjoint-based constrained topology optimization for viscous flows, including heat transfer, Engineering Optimization 45 (8) (2013) 941–961.

[38] J. Alexandersen, N. Aage, C. S. Andreasen, O. Sigmund, Topology optimisation for natural convection problems, International Journal for Numerical Methods in Fluids 76 (10) (2014) 699–721.

[39] A. A. Koga, E. C. C. Lopes, H. F. V. Nova, C. R. de Lima, E. C. N. Silva, Development of heat sink device by using topology optimization, International Journal of Heat and Mass Transfer 64 (2013) 759–772.

[40] G. Marck, M. Nemer, J.-L. Harion, Topology optimization of heat and mass transfer problems: laminar flow, Numerical Heat Transfer, Part B: Fundamentals 63 (6) (2013) 508–539.

[41] X. Qian, E. M. Dede, Topology optimization of a coupled thermal-fluid system under a tangential thermal gradient constraint, Structural and Multidisciplinary Optimization 54 (3) (2016) 531–551.

[42] S. Zeng, B. Kanargi, P. S. Lee, Experimental and numerical investigation of a mini channel forced air heat sink designed by topology optimization, International Journal of Heat and Mass Transfer 121 (2018) 663–679.

[43] J. H. Haertel, K. Engelbrecht, B. S. Lazarov, O. Sigmund, Topology optimization of a pseudo 3d thermofluid heat sink model, International Journal of Heat and Mass Transfer 121 (2018) 1073–1088.

[44] F. Dugast, Y. Favennec, C. Josset, Y. Fan, L. Luo, Topology optimization of thermal fluid flows with an adjoint lattice boltzmann method, Journal of Computational Physics 365 (2018) 376 – 404. doi:https://doi.org/10.1016/j.jcp.2018.03.040.
URL http://www.sciencedirect.com/science/article/pii/S0021999118302067

[45] K. Yaji, T. Yamada, M. Yoshino, T. Matsumoto, K. Izui, S. Nishiwaki, Topology optimization in thermal-fluid flow using the lattice boltzmann method, Journal of Computational Physics 307 (2016) 355 – 377. doi:https://doi.org/10.1016/j.jcp.2015.12.008.
URL http://www.sciencedirect.com/science/article/pii/S0021999115008244

[46] T. W. Athan, P. Y. Papalambros, A note on weighted criteria methods for compromise solutions in multi-objective optimization, Engineering Optimization 27 (2) (1996) 155–176.

[47] R. T. Marler, J. S. Arora, The weighted sum method for multi-objective optimization: new insights, Structural and multidisciplinary optimization 41 (6) (2010) 853–862.

[48] K. Khadra, P. Angot, S. Parneix, C. J-P, J. Numer. Methods Fluids 34 (2000) 651–684.

[49] T. DBOUK, F. PERALES, F. BABIK, R. MOZUL, A df-ibm/nscd coupling framework to simulate immersed particle interactions, Comput. Methods Appl. Mech. Engrg. 309 (2016) 610–624.

[50] M. P. Bendsoe, O. Sigmund, Topology optimization: theory, methods, and applications, Springer Science & Business Media, 2013.

[51] W. Jakob, C. Blume, Pareto optimization or cascaded weighted sum: A comparison of concepts, Algorithms 7 (1) (2014) 166–185.

[52] S. Nrgaard, O. Sigmund, B. Lazarov, Topology optimization of unsteady flow problems using the lattice boltzmann method, Journal of Computational Physics 307 (2016) 291 – 307. doi:https://doi.org/10.1016/j.jcp.2015.12.023.
URL http://www.sciencedirect.com/science/article/pii/S0021999115008426

[53] S. S. Rao, S. S. Rao, Engineering optimization: theory and practice, John Wiley & Sons, 2009.

[54] C. Hinterberger, M. Olesen, Industrial application of continuous adjoint flow solvers for the optimization of automotive exhaust systems, CFD & Optimization, Antalya, Turkey.

[55] H. K. Versteeg, W. Malalasekera, An introduction to computational fluid dynamics: the finite volume method, Pearson Education, 2007.

[56] K. Svanberg, A class of globally convergent optimization methods based on conservative convex separable approximations, SIAM J. Optim. 12 (2002) 555–573.

[57] T. Dbouk, J.-L. Harion, Performance of optimization algorithms applied to large nonlinear constrained problems, American Journal of Algorithms and Computing 2 (1) (2015) 32–56.

[58] O. Sigmund, J. Petersson, Numerical instabilities in topology optimization: a survey on procedures dealing with checkerboards, mesh-dependencies and local minima, Structural optimization 16 (1) (1998) 68–75.

[59] T. E. Bruns, D. A. Tortorelli, Topology optimization of non-linear elastic structures and compliant mechanisms, Computer Methods in Applied Mechanics and Engineering 190 (26) (2001) 3443–3459.

[60] O. Sigmund, Morphology-based black and white filters for topology optimization, Structural and Multidisciplinary Optimization 33 (4) (2007) 401–424.

[61] B. McKeon, C. Swanson, M. Zagarola, R. Donnelly, A. J. SMITS, Friction factors for smooth pipe flow, Journal of Fluid Mechanics 511 (2004) 41.

[62] S. Chen, G. D. Doolen, Lattice boltzmann method for fluid flows, Ann. Rev. of Fluid Mechanics 30 (2003) 329–364.